geomatics

MDPI

Article

Relationship Between Lithological and Morphometric Aspects of Mascasín Saline Watershed and Its Feeder Depositional Systems, San Juan and La Rioja Provinces, Argentina

Paula Santi Malnis [1,2,3,4,*] and Luis Martin Rothis [1,2,3,5]

[1] Consejo Nacional de Investigaciones Científicas y Técnicas (CONICET), San Juan CP 5400, Argentina; mrothis@unsj-cuim.edu.ar
[2] Departamento de Geología, Facultad de Ciencias Exactas, Físicas y Naturales, National University of San Juan Argentina, Rivadavia San Juan CP 5402, Argentina
[3] Instituto y Museo de Ciencias Naturales, Facultad de Ciencias Exactas, Físicas y Naturales, National University of San Juan Argentina, San Juan CP 5400, Argentina
[4] Centro de Investigación de la Geósfera y la Biosfera CIGEOBIO, Rivadavia San Juan CP 5402, Argentina
[5] Instituto de Geología, Facultad de Ciencias Exactas, Físicas y Naturales, National University of San Juan Argentina, Rivadavia San Juan CP 5402, Argentina
* Correspondence: psantimalnis@unsj-cuim.edu.ar

Abstract: Understanding the relationships among watersheds and derived depositional products is critical to developing analog studies with the rock record, especially for continental intermontane basins. Also, it is crucial to study river flood occurrences. Multivariate statistics analysis allows for the comprehension of the relationship among substrate, climate, and depositional products of the watersheds that feed the endorheic Mascasin Saline Basin, San Juan and La Rioja provinces, Argentina. Using a GIS platform, geomorphological, stratigraphic, morphometric, and structural analysis gave a dataset of variables for defining clusters. Under a similar climate, clustering analysis permits defining two main controls on watersheds and depositional products: parent rock composition and geological structures (faults and lineaments). The results underscore the critical role that lithology and structural controls play in basin morphometry and emphasize the need to quantify these variables for landscape evolution models.

Keywords: clustering; climate; transversal drainage systems; sedimentology

Academic Editor: Enrico Corrado Borgogno Mondino

Received: 19 September 2024
Revised: 19 November 2024
Accepted: 6 December 2024
Published: 30 December 2024

Citation: Santi Malnis, P.; Rothis, L.M. Relationship Between Lithological and Morphometric Aspects of Mascasín Saline Watershed and Its Feeder Depositional Systems, San Juan and La Rioja Provinces, Argentina. *Geomatics* **2025**, *5*, 1. https://doi.org/10.3390/geomatics5010001

1. Introduction

A depositional system, especially those governed by fluvial and alluvial environments, reflects through its deposits the characteristics of the watershed that feeds them [1]. Watershed morphometry and climate influence the capacity and competence of the trunk system, controlling the lithology and grain size of the resultant deposits [1,2]. Watershed parent rocks govern the composition of the derived deposits [3,4]. The slope depends on structures and tectonic deformation, impacting sedimentary processes [5–7]. In addition, tectonic uplift controls the pattern of the drainage network, which produces strike variations in sediment flows [8]. Channels adjust to uplift rates by both increasing their slope and narrowing their width [8]. To summarize, a basin's resultant deposits and facies architecture reflect the climate, morphometry, and composition of the parent rocks that control weathering, erosion, sediment transport, and depositional processes [9–12]. Unraveling these relations tends to result in different or even contradictory conclusions [2,13]. In modern environments, correlations between watershed aspects and resultant deposits are extensively discussed since similar morphometric and drainage responses occur under different climatic contexts [1,2,5,13–15].

After more than 100 years of research, most authors agree that under humid/wet conditions, more incision and rock exhumation occur than under dryer conditions [2,14–16]. Most research focused on quantifying the relationship between climate/climate change and basin morphometric parameters [14–17]. However, quantifying the underlying control that exerts the geologic substrate on landscape evolution and erosion rates remains unsolved [14,17,18]. To understand the influence of climate and geology on basin morphometry, principal component analysis applied in the Arabian Peninsula shows that shape parameters behave similarly in basins developed over volcanic rocks substrate [19]. Understanding the influence of parent rock composition, climate, and tectonics is crucial to interpreting the geological record in terms of paleobasin morphometry and paleoenvironmental evolution [9,10].

This paper uses an endorheic sedimentary basin to analyze the relationship between watershed morphometry, parent rock composition, and climate in the resultant drainage systems, depositional areas, and landscape organization. The Mascasín Saline Basin is an intermontane valley in Central Western Argentina's San Juan and La Rioja provinces [20] (Figure 1). Recently, this region has stood out as an important target of strategic mineral exploration. Still, their geological and geomorphological evolution characteristics are only briefly studied [21–24]. The climate in the Mascasín Saline Basin is semi-arid, locally transitioning to arid in the valley [25]. The Mascasín Saline Basin has an axial drainage system characterized by a fluvial distributary pattern that transitions to saline according to local climatic conditions. Feeder transversal drainage systems of the Saline are those of the alluvial environment, like alluvial fans and distributive fluvial systems [26]. The Mascasín Saline Watershed exhibits various rock types from plutonic, sedimentary, metamorphic, and volcanic. Also, only some transversal drainage systems superficially reach the Saline's depocenter, developing high-aggrading environments [25], while the others remain on the Saline coast. When observing the Saline valley, the following questions arise: Is there any substrate control to favor the production of a great amount of sediments to create a highly aggrading depositional system? Why do only some feeder systems reach the Saline under similar climatic conditions? To summarize, what are the main controls on the Mascasin Saline landscape? This paper analyzes the relations among morphometric parameters, watershed parent rock composition, and climate to understand the geomorphological relation between source areas and deposits that may control exogenous processes.

Different approaches, such as geomorphologic, stratigraphic, and multivariate cluster analysis, study the relation among parent rock composition, morphometric parameters, and depositional areas. A GIS platform allows the study to be performed using satellite images to obtain watershed morphometry and climate data. Multispectral satellite images help in geological unit digitalization to characterize the parent rocks of each drainage basin [27]. Once the variables that represent morphometry, climate, and parent rock composition from each drainage basin were defined, multivariate analysis in R studio was applied. The results are the basis for a first approach to quantifying substrate geology control on drainage basin morphometry.

2. Geological Setting

The Macasín Saline is located in the broken foreland of the Western Pampean Ranges geological province (Figures 1 and 2) [20,21,28]. The Saline Watershed's geological units exhibit a diverse lithologic composition among sedimentary, igneous, and metamorphic rocks. From north to south in the western border of the basin, the northernmost part of the watershed is in the Vilgo range and the Barrancas Coloradas, which have mostly Triassic sedimentary rocks of the Ischigualasto-Villa Union Basin. Then, the Valle Fértil–La Huerta–Imanas ranges are composed of crystalline basement rocks represented by the Valle Fértil Complex and Triassic–Jurassic sedimentary rocks of the Marayes-Carrizal Basin.

Toward the south, in the Leyes Low Hills until the Guayaguas Hill, the sedimentary rocks of the Marayes-Carrizal Basin continue, and the Cretaceous rocks of the El Gigante Group appear [27,29,30]. In the eastern border, the Chepes ranges are Ordovician grani-toids of the Chepes Igneous Complex and migmatites of the Olta metamorphic complex. In smaller amounts, sedimentary rocks outcrop in the western piedmont of the Chepes range. Neopaleozoic rocks such as the Malanzan Formation and the La Colina Formation and younger Mio–Pliocene rocks of the Los Llanos Formation also outcrop [30,31].

The Mascasin Saline is in the northern part of the Las Salinas Basin [21]. The Las Salinas Basin was interpreted through subsurface data as a series of asymmetric anticlines trending north-northeast, with their western flanks truncated by reverse faults parallel to the anticline axis [21,23,24]. The Las Salinas Basin is believed to have an extensional origin, shifting to a compressional regime by the end of the Cenozoic due to Andean orogeny, which caused reverse faulting that uplifted Mesozoic and Neogene rocks to the surface [21,23,24]. The Marayes Fault System, with Quaternary activity, is defined in the eastern foothills of the La Huerta range [32].

Structural and neotectonic studies in the southwestern portion of the La Huerta range defined several fault systems that could control the drainage systems in the study area. These fault systems have NW, NE, EW, and ESE orientations. The most conspicuous have an NW orientation, coinciding with the regional structure of the Valle Fértil mega fracture (Figure 1) [29,30,33,34]. In the eastern foothills of the La Huerta range, structures with neotectonic activity-caused anomalies in drainage systems, and these structures have an NW orientation within the Marayes fault system [32].

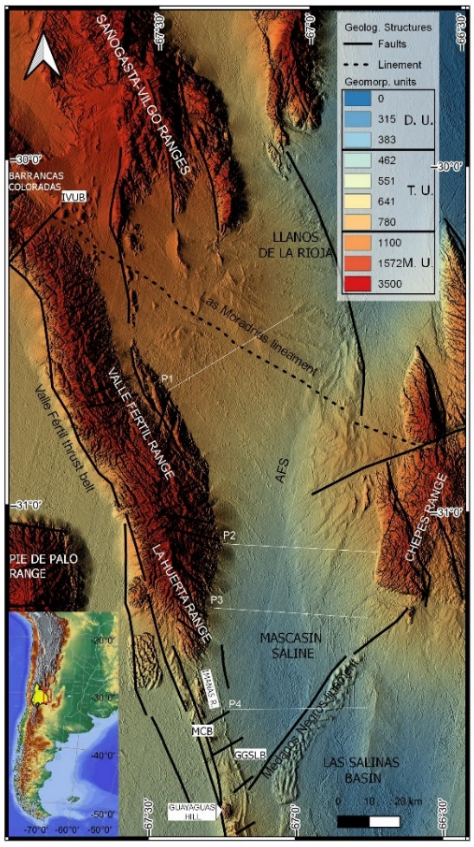

Figure 1. Location map of Mascasín Saline Basin. Shaded relief map where geomorphological units [32] shown by heights. D.U., depression unit; T.U.: transition unit; M.U.: mountain unit; AFS: axial fluvial system. Geologic structures identified in literature [23,30,32,34] in solid line, proposed structure in this paper is dashed lines. IVUB: Ischigualasto Villa Union Basin; MCB: Marayes−Carrizal Basin; GGSLB: the Gigante Group of the San Luis Basin; AFS: Axial Fluvial System. P1-P4 topographic profiles.

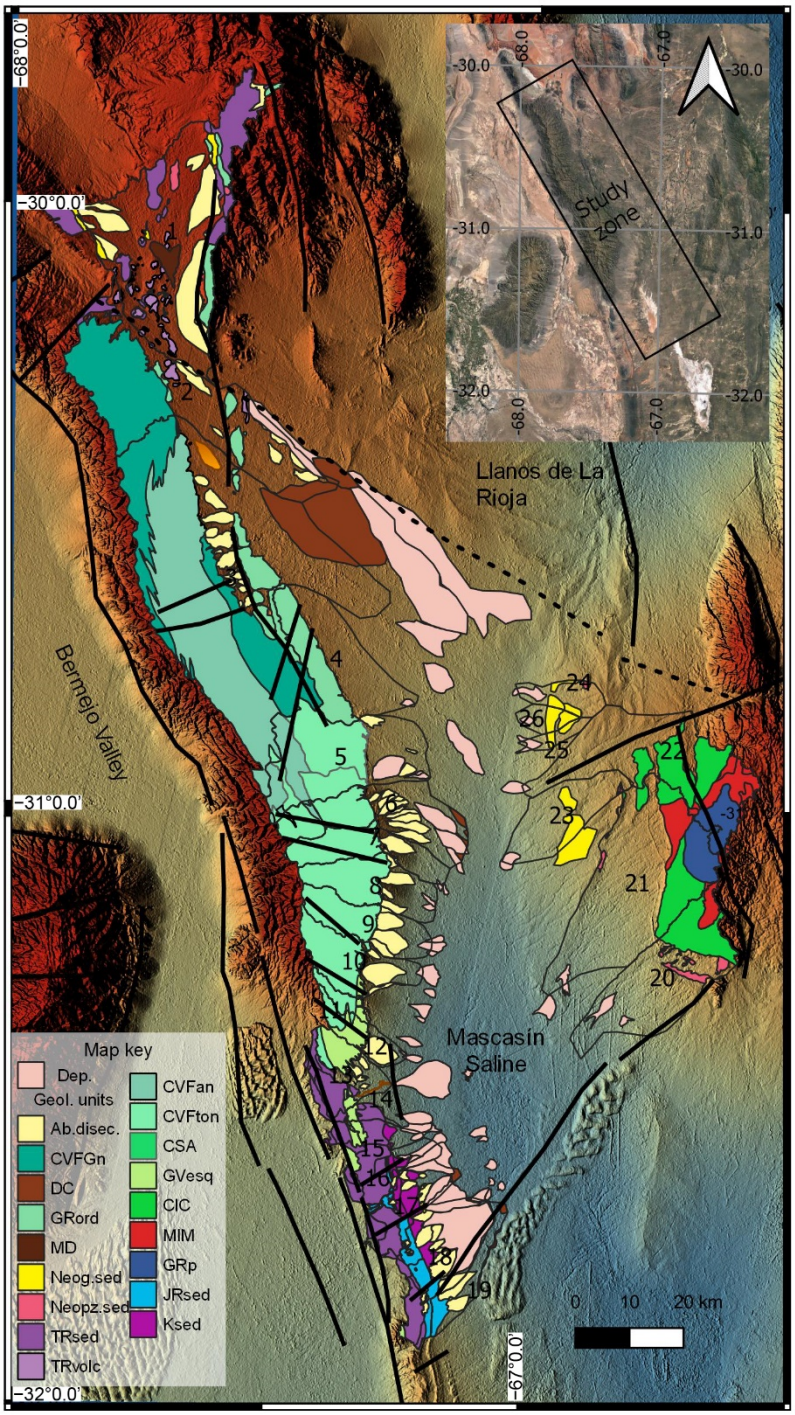

Figure 2. Geological units identified in Mascasin Saline Watershed. Dep. refers to depositional bodies. Acronyms used: Neopz.: Neopaleozoic; TR: Triassic; JR: Jurassic; K: Cretacic; Neog.: Neogene; sed.: sedimentary; volc.: volcanic; ton: tonalite; an: amphibolite; esq: schist; Fl-eol: fluvial eolian; Ab. disec.: dissected fans; MD: eolian dunes field; DC: coastal dunes and valley dunes; GRp: porphyric granitoids; GRord: ordovician granitoids; CIC: Chepes Igneous Complex; CSA: San Agustin Complex; CVFGn: Valle Fertil Complex gneiss; CVFan: Valle Fertil Complex amphibolites; CVFton: Valle Fertil Complex tonalites; GV: Villarcan Gneiss; MIM: migmatites. Numbers 1 to 26 refers to each drainage basin ID.

2.1. Geomorphologic Setting

The Mascasín Saline Basin is in the intermontane valley known as the Gran Bajo Oriental, which borders the provinces of San Juan and La Rioja [30]. Three morphostructural units were defined in the western portion of the study area: the mountain, the transition,

and the depression units [32]. The mountain unit corresponds to the highest elevation landscape elements (Sierra de la Huerta, 2060 m above sea level, Figure 1) formed by crystalline rocks of the Valle Fértil Complex. It has an NW-SE orientation, with decreasing elevations from north to south (from 2060 to 500 m above sea level) and an asymmetrical profile from east to west. The transition unit corresponds to the eastern piedmont of the Sierra de la Huerta and Imanas and extends to the depression unit, formed by seven alluvial levels (Figure 1). The alluvial levels in the northern portion of the study area have darker tones related to the mafic composition of the source rocks, composed of amphibolites, gneisses, schists, and basic intrusive rocks. In contrast, those in the southern portion have lighter tones and are composed of quartz, schists, amphibolites, and granodiorites. The current alluvial level has amphibolites, quartz, schists, and granodiorites. The depression unit consists of the Mascasín salt flat, oriented N-S, 29 km long, and 8 km wide, composed of fine sediments and salts, located in the central-southern portion of the valley (Figure 1). In the depression unit, eolian dunes develop in the coastal zone, composed of reworked material from the salt flats [22].

The eastern portion of the study area presents a similar landscape since the salt flat is surrounded by the Sierra de Chepes, mainly formed by the Lower Paleozoic Olta Metamorphic Complex and the Chepes Igneous Complex. Its western piedmont displays Quaternary alluvial fans and eolian longitudinal and transverse dunes on the Saline coast. To the south, the Médanos Negros develops, separating the Mascasín Saline from the southern portion of the Las Salinas Basin [20,22,30].

Landscape shapers are dominated by physical weathering, which through thermoclastism, is the principal factor that produces rock disaggregation [20,35]. Fluvial and eolian processes are the principal factors shaping the landscape in the study zone [36].

2.2. Climate

Paleoclimate in the Western Pampean Ranges of San Juan reveals a persistent seasonal semi-arid to arid climate after the Pliocene and during the Quaternary [22,28]. On the other hand, the exhumation of nearby ranges is mostly tectonically driven, with a similar topography from Paleogene times (Pie de Palo Range) [28,37,38] or from the Pliocene (Los Llanos Ranges [39]. During the Late Pleistocene and Holocene, glaciation and cryogenic ambient occurred in the Andes Cordillera highlands (above 4000 m asl) while pronounced aridity intervals favor draas forming in the broken foreland [22]. In the last 1000 yr, reactivation of the Médanos Negros suggests dryer conditions than now, with climatic improvement (producing similar current conditions) between 1400 and 800 years BP [22,40,41].

Current climatic data near the study area was obtained from the National Weather Service (SMN) database [42] and the INTA website [43]. Only one station close to the study zone appears currently available on the SMN website, the Chamical station. Climatic data from the El Portezuelo station, located in the Sierra de Chepes and Chepes locality (currently unavailable), are reported from previous studies [25]. Data from these meteorological stations report the seasonal behavior of the climate, with the highest amount of rainfall occurring in December, January, February, and March, while in winter, it is scarce. The mean rainfall for Chepes and Chamical localities are 359 mm and 462 mm, respectively [44]. According to Köppen classification, the study zone shows semi-arid and arid climate, BWwha for the valley (hot arid), BSwka for the western ranges (steppe cold semi-arid), BSh for the eastern ranges (steppe hot semi-arid; [44–46]). Untimely and torrential rains occur during summer, and in the western ranges, winter is colder. In all the regions, evapotranspiration exceeds rainfall [45,47]. The Global Aridity Index and the INTA Aridity Index classify the region as having an arid to semi-arid climate [43]. Congruently, the TRMM model showed the mean annual precipitations below 500 mm and above 200 mm [48]. The climate in the study zone

gradually changes from one geomorphological unit to the other. It is semi-arid to arid in the mountain and transition units, while the depression unit is mostly arid.

3. Materials and Methods

Drainage basins were defined using 30 m digital elevation models downloaded from the National Geographic Institute [49]. Through the Basic Terrain Analysis routine of Terrain Analysis library tool of the SAGA GIS software, drainage basins and the Strahler order were automatically determined [50,51]. Then, Google and Bing aerial images on QGIS Software 3.16 (Google images of 2015, [52,53]) enabled the inspection and re-definition of the boundaries of the drainage basins and drainage nets. For the Sierra de la Huerta and Imanas ranges, drainage basins from [35] were used. To standardize measurements based on the drainage basin channel network, those channels from the third Strahler order were considered. Watersheds were organized according to the rivers that reached the piedmont and may superficially feed the basin. The attribute table of the drainage basin contains the following parameters: ID, maximum height (H, m), and minimum height (in the spillway, h, m). In the field calculator on QGIS area (A, km^2), perimeter (P, km), total length of streams (Tsl, km), and basin length (L, km) were obtained [54]. Then, morphometric parameters were measured on a spreadsheet following the formulas (Table 1).

Table 1. Morphometric parameters used in this work.

Parameters	Formula	Reference
Drainage density (Dd)	$Dd = Tsl/A$	Horton 1945 [54]
Form factor (Ff) [1]	$Ff = A/L^2$	Horton 1932 [55]
Circularity ratio (C)	$C = 4\pi A/P^2$	Miller 1953 [56]
Elongation ratio (Re)	$Re = (\sqrt{4A/\pi})/L$	Schumm 1956 [57]
Basin relief (Hr)	$(H-h)/1000$	Hadley and Schumm 1961 [58]
Relief ratio (Rr)	Hr/L	Schumm 1956 [57]
Compactness coefficient (Kc)	$0.28(P/\sqrt{A})$	Gravellius 1914 [59]
Melton ruggedness number (MRN)	$Hr/A^{0.5}$	Melton 1957 [6]

[1] Also expressed as Rf.

Since rainfall is an essential variable in weathering and sediment transportation, the mean annual precipitation [mm/year] across South America obtained from the dataset of the Tropical Rainfall Measuring Mission (TRMM 3B43) served as a variable that represents climate in this study [48]. This model spans the period from 1998 to 2015, and the precipitation values of the studied basins agree with the data reported by the meteorological stations [25,42].

Depositional areas were also digitized through a photogeological and geomorphological survey, considering only deposits under current climatic and tectonic conditions. Stratigraphic units in the watersheds were defined using multispectral images, geological units were defined by cartography, and databases elaborated in previous studies pursued in the Ischigualasto-Villa Union and Marayes-Carrizal basins [27,60,61].

The geological composition of each drainage basin was obtained through advanced digitization tools such as extraction and intersection (Figure 2). Five classes grouped the lithological characteristics of the source areas: igneous rocks, metamorphic rocks, sedimentary rocks (including volcanic rocks), eolian dunes, and incised alluvial fans. Volcanic rocks were included within sedimentary rocks as they are outcroppings intercalated with the sedimentary rocks of the Ischigualasto-Villa Unión Basin. The sedimentary rocks class comprises the eolian dunes and incised alluvial fans classes. Thus, three classes composed the source areas: sedimentary, metamorphic, and plutonic igneous rocks. The polygon areas represent drainage basins' different lithologies, measured using the field calculator (Table 2). The data obtained from the basins were exported to a data spreadsheet to obtain the representative

percentage of each basin. The sum of the three variables, %IG + %Met + %RSED, equals 100%. Then, in Rstudio, using the ggplot and ggtern packages, the three classes gave a ternary diagram, which visually represents the lithologic composition of the basins [62,63].

Table 2. Geological units class defined in study. Figure 2 is spatial distribution. Neopz.: Neopaleozoic; TR: Triassic; JR: Jurassic; K: Cretacic; Neog.: Neogene; sed.: sedimentary; volc.: volcanic; ton: tonalite; an: amphibolite; esq: schist; Fl-eol: fluvial eolian; Ab. disec.: dissected fans; MD: eolian dunes field; DC: coastal dunes and valley dunes; GRp: porphyric granitoids; GRord: ordovician granitoids; CIC: Chepes Igneous Complex; CSA: San Agustin Complex; CVF: Valle Fertil Complex; Gn: gneiss; GV: Villarcan Gneiss; MIM: migmatites.

Geological Unit	Description	Material	Class
Neopz.sed	Paganzo Group	Mudstones and sandstones	%RSED
TRvolc	Baldecitos Fm.	Alkaline basalts	%RSED
TRsed	Talampaya, Chañares, Los Colorados Fms. Carrizal, Quebrada del Barro and Qda. del Puma Fms.	Sandstones and mudstones Mudstones, sandstones, and conglomerates	%RSED %RSED
JR sed	Balde de Leyes and Rancho Grande Fms.	Mudstones and sandstones	%RSED
Ksed	El Gigante Group	Conglomerates, mudstones, and sandstones	%RSED
Neog. sed	Quebrada del Médano, Los Llanos Fms.	Sandstones, mudstones, and pyroclastics	%RSED
Fl-eol	Ab. Fluvial dep. with eolian acum.	Sandy sediments	%RSED
Ab. disec	Guayapas and Catinzaco Fms.	Gravel, sands	%RSED
MD	Pagancillo Dunes field	Sands	%RSED
DC	Coastal dunes (Pleist.–Holoc)	Sand to silt	%RSED
GRp	Granitoids	Porphiric granitoids	%IG
GRord	Cerro Blanco Fm.	Granitoids	%IG
CIC	Chepes Igneous Complex	Granitoids	%IG
CSA	San Agustin Complex	Granites, norites, and tonalites	%IG
CVFton	Valle Fertil Complex	Tonalites, diorites	%IG
CVFan	Valle Fertil Complex	Amphibolites	%MET
CVFGn	Valle Fertil Complex	Granodioritic gneiss	%MET
GVesq	Villarcan Gneiss	Schist, gneiss	%MET
MIM	Olta Complex	Migmatite	%MET

A dataset of 26 basins characterized for morphometric parameters, depositional areas, parent rock composition, and precipitation values was created (Table 3). With this dataset in RStudio, a cluster analysis was performed in a script with the following packages [63–74]: dplyr, sandwich, pastecs, carData, e1071, NbClust, mvtnorm, ggplot2, corrplot, haven, RcmdrMisc, rstatix, factorextra (Supplementary Materials). A clustering analysis is an unsupervised technique that consists of cluster data based on the distance among observations. If two observations in a dataset have a closer behavior or pattern, their distance will be smaller. In this case, both Euclidean and Manhattan distances compute distance calculation. Outliers could affect the Euclidean distance more, while Manhattan distance may not [59]. Also, the different data measurement units can affect Euclidean distance [75,76]. Finally, Centroid and Ward methods were used for cluster definition [75,76]. Dendrograms were built using quadratic Euclidean and Manhattan distances, applying a hierarchical

clustering technique through Centroid and Ward methods. The best partition of the matrix was applied to define the clusters, and then, with these data, clusters were built.

Table 3. Shapiro–Wilk normality test.

Variable	W	*p* Value [1]
Area_cca	0.72954	0.01308
Perim_cca	0.82266	0.0004346
Clima	0.89842	0.01443
Dd	0.8226	0.0004377
%IG	0.76409	4.577×10^{-5}
%Met	0.69072	3.968×10^{-6}
%RSED	0.70887	7.029×10^{-6}
Deparea	0.64605	1.051×10^{-6}
L (km)	0.91463	0.03371
Kc	0.88254	0.006517
C	0.97907	0.8535
E	0.93599	0.1077
Ff	0.89828	0.01434
Rr	0.79359	0.0001373

[1] p value > 0.05 is normal.

4. Results

The Mascasín Saline drainage basin has an irregular (triangle) morphology and covers an area of 7618 km^2 (Figure 2). The drainage basin extends from the northwest end of the Vilgo range, Barrancas Coloradas, and the northern end of the Valle Fértil range. It extends west to the Valle Fértil–La Huerta–Las Imanas ranges, and continues southwest until it reaches the Lomas de Leyes Low Hills. The Médanos Negros dunes field borders it by the south, with the Chepes range towards the east.

4.1. Parent Rocks Composition

The drainage basins of the Mascasín Saline were organized according to the rivers that flow into the valley (Figures 2 and A1). A total of 26 basins were defined, whose general characteristic is that most of the fluvial channels disappear in the piedmont due to infiltration into the sandy sediments that cover the entire valley.

Basin ID1 encompasses the Las Moradrias and Punta del Médano rivers, which come from the Pagancillo basin at the southern end of the Sierra de Vilgo and the Barrancas Coloradas (Figure 2). The composition of the rocks that make up this basin includes Triassic sedimentary rocks of the Ischigualasto-Villa Unión Basin (TRsed, Table 2). Also contributing are Neopaleozoic (Neopz.sed) and Neogene sedimentary rocks (Neog.sed), Ordovician granitoids (GRord), and alkaline basalts (TRvolc, Table 2). Deposits of inactive ancient fans, dune fields, and ancient coastal dunes form a significant part of the drainage basin. Basin ID2 originates from the northern end of the Valle Fértil range, and its composition mainly consists of granodioritic gneisses of the Valle Fértil Complex (CVFGn). Basin ID3 belongs to the Usno-Valle river, including the central portion of the Valle Fértil range (Figure 2). Basin ID3's composition is crystalline rocks of the Valle Fértil Metamorphic Complex (CVFan-CVFGn), such as amphibolites, granodioritic gneisses, and tonalites, as well as Ordovician granitoids of the Cerro Blanco Formation (GRord). Sediments formed by ancient fans are part of the basin of these rivers. Basin ID4 is formed by the granitoids of the Cerro Blanco Formation and the Valle Fértil Complex. Basin ID5 corresponds to the Las Tumanas and Astica rivers in the central-southern portion of the Valle Fértil range. The composition of drainage basin ID5 is plutonic igneous rocks, distinguished by the Valle Fértil and San Agustín complexes (CSA). Basins ID6 to ID12 occupy the Huerta Range and involve the Huerta and Las Tuscas

rivers. The dominant composition is diorites and quartz-bearing tonalites of the Valle Fértil Complex, and secondarily include metamorphic rocks of the Villarcan Gneiss (GVesq).

Basin ID13 shows more differences in its composition than those mentioned above. The Papagayos River is the Saline's central detrital sediment feeder system. Mesozoic sedimentary rocks like greenish and tuffaceous sandstones and red beds are the dominant source composition of the basin (TRsed, JRsed, Ksed), followed by foliated metamorphic rocks (GVesq).

Basins ID14 to ID17 are in the southwestern part of the Mascasin Saline Basin and include the Las Imanas-Salada and Bajos del Estanque rivers, involving the Leyes Hills and the Sierra de las Imanas. The dominant composition is clastic sedimentary rocks. Siltstones, sandstones, eolian sandstones and conglomerates form the highest part of the Leyes Hills, while the lowest part comprises shales and gypsum deposits (TRsed, JRsed, Ksed). Basins ID18 and ID19 are located at the southern end of the Leyes Hills up to the Guayaguas Hill, and the primary river is the Narvaez River, which reaches the coastal edge of the Saline flat. The composition of these basins is similar to the above-mentioned (Basin ID14–17) and to a lesser extent includes the Médanos Negros dunes field.

To the east, the source areas belong to the Chepes Range, where basins ID20 to ID26 are located. Basins ID20 and ID21 are located southwest of the Chepes Range, composed of the Chepes Igneous Complex (CIC) and Neopaleozoic sedimentary rocks (Neopz.sed). Basin ID22 develops in the northwestern portion of the Chepes Range, and its main river is the El Portezuelo River. The composition of the rocks of Basin ID22 includes granitoids, porphyritic granitoids, and migmatites (MIM). On the western piedmont of the Chepes Range, Basin ID23 comprises Neogene sedimentary rocks and the CIC. Basins ID24-ID26 develop on hills in the piedmont, and their composition includes Neopaleozoic and Neogene sedimentary rocks.

According to Figure 3, most drainage basin composition is represented in more than 80% for one class. There are also mixed compositions where the dominant class has a 70% and 80% representation between igneous and metamorphic rocks, and sedimentary and metamorphic rocks, respectively. Only Basin ID1 presents a mixed composition between sedimentary and igneous rocks, with igneous rocks being less than 20% representative. Basins ID12 and ID13 present a mixed composition, with 50% and 60% between metamorphic and igneous rocks, and between sedimentary and metamorphic rocks, respectively.

A

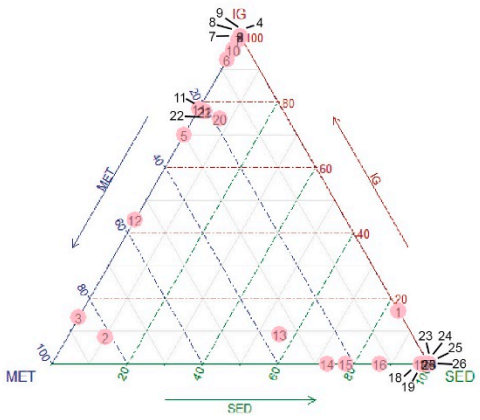

B

ID	%IG	%Met	%RSED
1	16	0	84
2	9	83	8
3	12	84	0
4	100	0	0
5	70	30	0
6	93	7	0
7	99	1	0
8	100	0	0
9	100	0	0
10	96	4	0
11	78	22	0
12	44	56	0
13	0	0	0
14	0	27	73
15	0	22	78
16	0	13	87
17	0	1	99
18	0	2	98
19	0	0	100
20	75	18	7
21	77	21	2
22	77	21	2
23	0	0	100
24	0	0	100
25	0	0	100
26	0	0	100

Figure 3. Composition of parent rocks of Mascasín Saline. (**A**) Ternary diagram showing composition distribution of 26 basins comprising Mascasín Saline Watershed. Pink points are each basin's position, labeled from 1 to 26 with the basin ID. IG: igneous rocks composition; MET: metamorphic rocks composition; SED: sedimentary rocks composition. (**B**) Composition values of each basin. Each corner of the ternary diagram representes the 100% of each composition.

4.2. Morphometry

Of the 26 basins, 19 are on its western margin and 7 on its eastern margin. Most basins develop towards the north of the depocenter. Those basins on the northwestern margin that drain in an NW-SE direction, have significant areal extension (ID1–3). In contrast, those found in the middle section that drain in the W-E direction, have a minor areal extension and are very elongated (ID4-12; Figures 2–4). On the other hand, the basins on the eastern margin of the valley drain mainly in an NE-SW direction (ID20–26). These basins drain to the axial river, which has an NE-SW direction. The basins in the southern part drain in an SW-NE direction, straight to the salt flat, with smaller sizes (ID13–19).

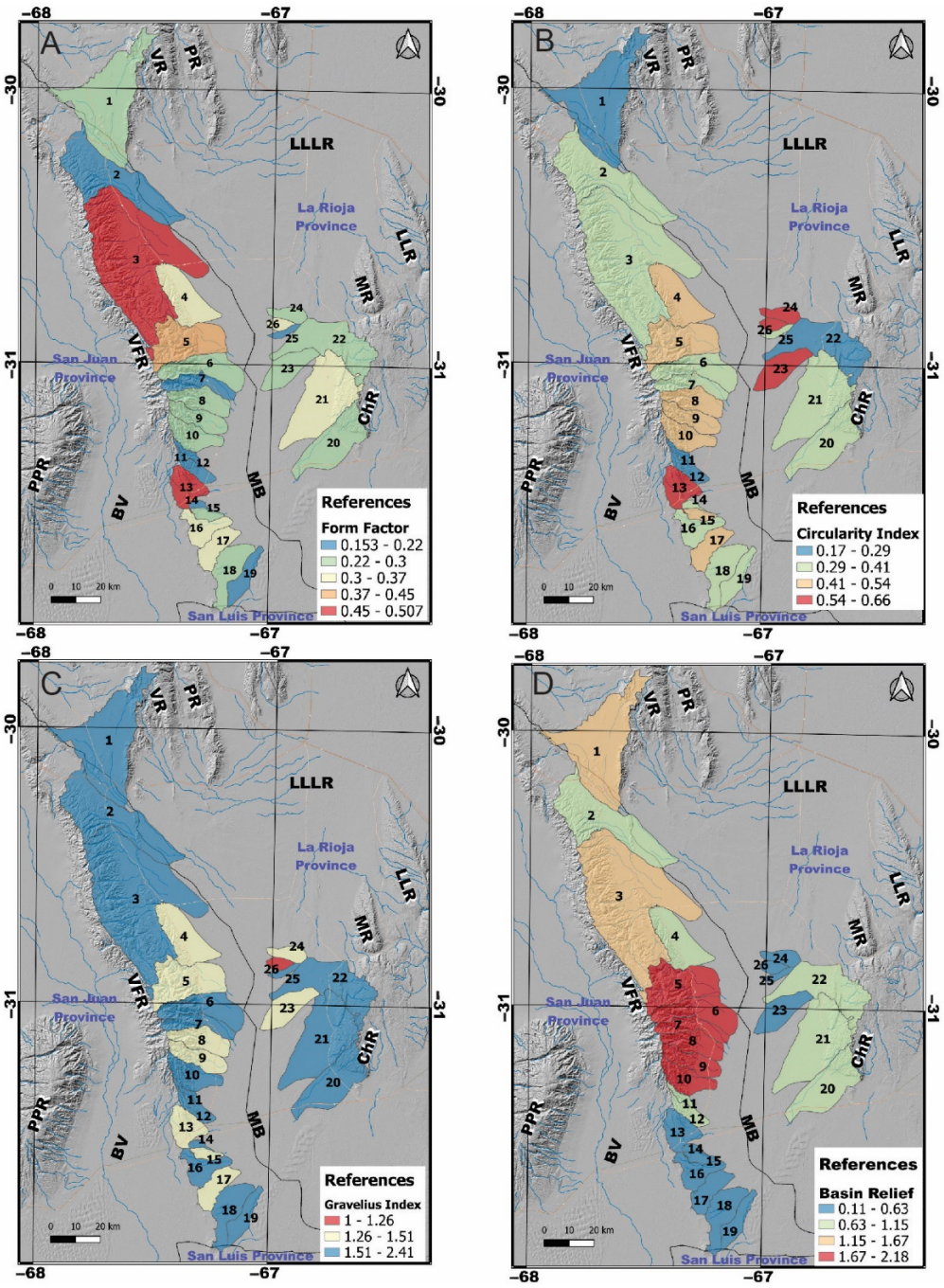

Figure 4. *Cont.*

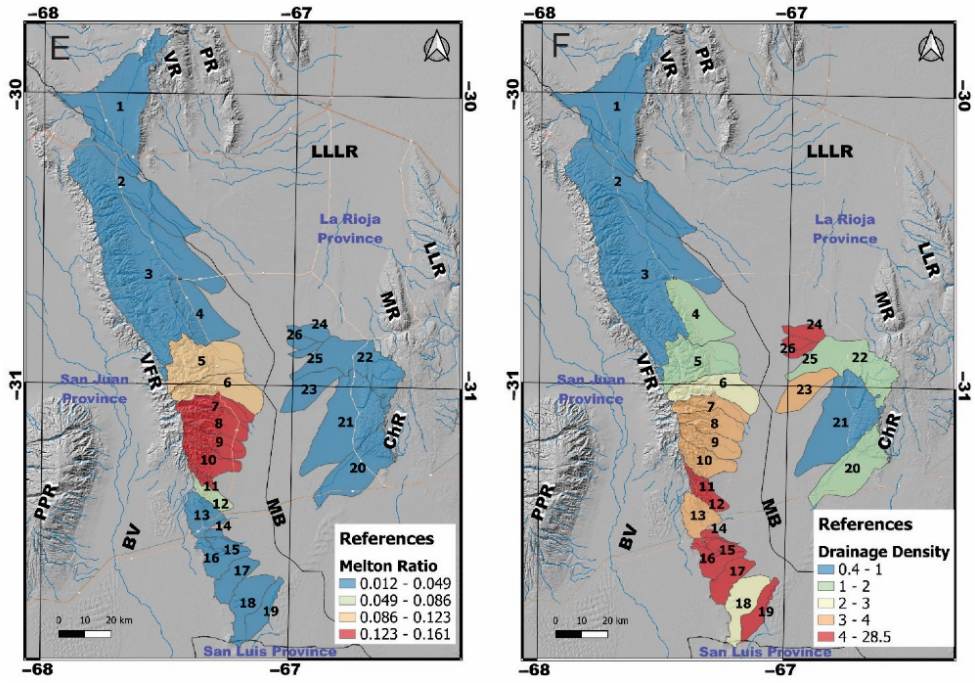

Figure 4. Heatmaps comparing behavior of morphometric parameters in 26 basins under study. Number labelled from 1 to 26 are basins IDs'. (**A**) Form factor. (**B**) Miller Circularity index. (**C**) Gravellius Index. (**D**) Basin Relief. PR: Paganzo Range, VR: Vilgo Range, LLLR: Llanos de la La Rioja, LLR: Los Llanos Range, MR: Malanzán Range, ChR: Chepes Range, MB: Mascasin Basin, VFR: Valle Fertil Range, BV: Bermejo Valley, PPR: Pie de Palo Range. Heatmaps comparing behavior of morphometric parameters in 26 basins under study. (**E**) Melton Ruggedness ratio. (**F**) Drainage density. PR: Paganzo Range, VR: Vilgo Range, LLLR: Llanos de la La Rioja, LLR: Los Llanos Range, MR: Malanzan Range, ChR: Chepes Range, MB: Mascasin Basin, VFR: Valle Fertil Range, BV: Bermejo Valley, PPR: Pie de Palo Range.

Different morphometric parameters have been used to characterize each basin and determine their differences. Taking into account the form factor, the observed basins mostly present values less than 0.3, indicating elongated to very elongated morphologies. Basins ID3 and ID13 present morphologies slightly widened (Figure 4A,B).

The Miller circularity coefficient has a maximum value of 0.66. However, most of the basins have values less than 0.5, which indicates elongated to very elongated morphologies. The Miller circularity coefficient shows the lowest values to those basins parallel to oblique NW-SE structures that bound the Mascasin Saline Basin (Figure 4B). On the other hand, the compactness coefficient Kc in most of the basins presents values greater than 1.26, which indicates oval–oblong to oblong–rectangular morphologies in coincidence with the rest of the calculated shape indices (Figure 4C). The elongation radius values are less than one, giving results similar to the form factor. This indicates that the basins have elongated morphologies. The highest values are found in the extreme north and south of the Valle Fértil range, in basins ID3, ID5, and ID13. Considering morphological indexes and the substrate, the geological structures control these parameters. The largest basins (BID 1–3) show a dominant extension towards the principal structure (NW-SE trend). In contrast, the basins in the central-western region display a W-E control, and those of the southwestern and eastern margin of the basin have an SW-NE extension. Basin ID13 outstands in the parameters as the most rounded and wide.

The highest values of the unevenness, relief ratio, and Melton roughness index are in the central sector of the Valle Fértil range (Figure 4D,E). Igneous rocks mainly comprised basins in this sector, and alluvial fans characterize the eastern foothills of the Valle Fértil range. Conversely, lower values of the indexes are given in basins where sedimentary rocks dominate, and fluvial distributary landforms appear in the transition unit.

On the other hand, the drainage density of the northwestern margin (ID1–3) has moderate to low values (Figure 4F). These values are because basins ID1–3 have large areas, and the drainage density is inversely proportional to this parameter. In addition, the parent rocks are another factor that control drainage density. Basins of the central-western margin of the Saline, mainly developed on igneous rocks, present high values. Meanwhile, those in the southern and northeastern margins, dominated by sedimentary rocks, have very high drainage density values. A more significant structural development of the drainage network, and a greater erosion capacity, can explain these behaviors.

4.3. Cluster Analysis

A multivariate statistical analysis (R script in Supplementary Materials) was applied to evaluate the relations among morphometric, compositional, and climatic variables of watersheds on depositional products (Figure A2). A cluster analysis aims to define an unknown number of groups in a dataset, where data contained in each cluster is homogeneous and different from other clusters [77]. Before performing the cluster analysis, an exploratory data analysis allows a visual comparison of the data relationship.

The variables defined for this study are listed in Table 3. The variable "Clima" refers to mean annual precipitation in mm. A visual inspection of the 15 variables through scatter plots shows a linear relation only between perimeter and area, elongation ratio and form factor, and compaction and circularity index, as expected (Table 1). The histograms and the Shapiro–Wilk test allowed for the evaluation of the normality of each variable (Figure A3, Table 3). The histograms showed asymmetric data and generally no normal distributions. The Shapiro–Wilk test revealed that only the variables C (circularity ratio) and E (elongation ratio) have normal distributions with a *p*-value greater than 0.05 (Table 3). According to boxplots, the dataset shows some outliers in the variables Area, Perim, %Met, Deparea, Dd, and derived parameters like L, Kc, and Ff (Table 4, Figure A3). The dataset was inspected to verify that the outliers were unrelated to possible data collection errors and accused genuine outliers.

Table 4. Outliers identification.

Variable	Outliers	Basin ID
Area_cca	1535	3
Perim_cca	252–246	1–3
%Met	83–84–56	2–3–12
Deparea	204–166	1–2
Dd	19.28–28.46–19.92	11–14–25
Ff [1]	0.51–0.50	3–13

[1] Also expressed as Rf. Outliers identification using boxplot.stats function in Rstudio. Outliers values and basin IDs' are separated by hyphens.

4.3.1. Correlation Matrix

The correlation matrix allows us to quantify the relationship among variables. These relationships are observable from the dataset's visual inspection and the performance of the morphometric parameters, for example, in the geological context. Since the dataset included different units of measurement, it was scaled to avoid its influence on the correlation. The visual inspection of each variable and the Shapiro tests reported that several variables do not have a normal distribution. Thus, the Spearman algorithm led to obtaining a correlation matrix. In addition, the covariance matrix was obtained to apply a cluster analysis [77]. The covariance matrix shows high and positive correlation values between variables with an intrinsic relationship, such as area, perimeter, and length of the basin, as well as the parameters derived from these (Figure 5).

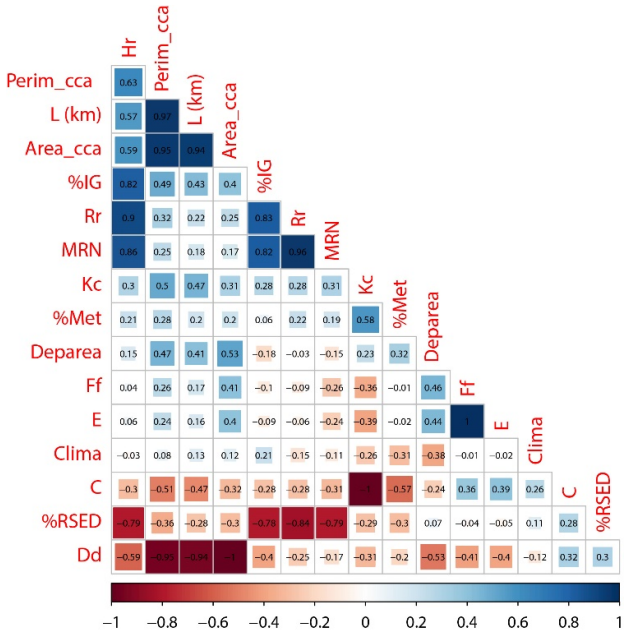

Figure 5. Correlation matrix. Variables labeled as: Hr: basin relief; Perim_cca: basin perimeter; L (km): basin length. Area_cca: basin area; %IG: parent rocks of igneous dominant lithology; Rr: relief factor; MRN: Melton ruggedness number; Kc: compactness coefficient; %Met: parent rocks of metamorphic dominant lithology; Deparea: area of active depositional products of each basin main river; Ff: form factor; E: elongation ratio; Clima: mean annual precipitation; C: circularity ratio; %RSED: parent rocks of sedimentary dominant lithology; Dd: drainage density.

The variable %IG shows a high positive correlation with Hr and moderate with perimeter, length, area, and the MRN index. So, a higher proportion of igneous rocks in the source areas generates basins with more relief and would be prone to generating sedimentary processes with non-fluid flows. However, all basins have MRN values below the threshold between fluid and non-fluid flows (0.25 [6]). Variable %IG has a positive but moderate to low correlation with the Kc index and precipitation variables. The variable %IG has a robust negative correlation with the variables %RSED, indicating that these two types of rocks are infrequent in the same basin and with drainage density, meaning that a higher proportion of igneous rocks results in a lower density of the drainage network. There is also a moderate to weak negative correlation with the circularity coefficient.

At the other end of the matrix is the variable %RSED, which has strong negative correlations with basin relief, the Rr relief ratio, the proportion of igneous rocks, and the MRN index. Thus, basins with more sedimentary rocks develop in regions with lower height relief. The variable %RSED shows a positive and moderate to weak correlation with the circularity coefficient and does not present a significant correlation with precipitation and the depositional area. The variable %RSED has negative and moderate correlations with the perimeter, basin length, basin area, compaction coefficient Kc, and metamorphic rocks. The variable %Met positively and moderately correlates with the depositional area and the compaction index. Thus, a higher proportion of metamorphic rocks in the basins may be associated with larger depositional areas. It also shows positive and moderate to low correlations with basin relief, area, perimeter, basin length, and MRN. Finally, the depositional area shows positive and moderate correlations with the shape factor and the elongation ratio, as well as with the basin area and perimeter, and a positive but low correlation with the relief. Dep.area displays a moderate negative correlation with the precipitation variable, the compaction index, and the drainage density. Finally, the drainage density variable has a positive and moderate correlation with the presence of sedimentary rocks and the C index. Negative and moderate to low correlations exist with precipitation,

Rr, %Met, and the MRN index. It shows negative and moderate correlations with relief, %IG, Kc, Ff, Re, and the depositional area, and strong negative correlations with relief, perimeter, channel length, and basin area (since the area defines it).

Precipitation, in the middle of the correlation matrix diagram, shows a low correlation with most variables. It shows a low and positive correlation with %IG and the C index and moderate to low negative correlations with the depositional area, Kc, and %Met.

4.3.2. Clustering

The Euclidean and Manhattan distances in the data matrix were measured to obtain dendrograms. Visual inspection of the dendrogram allows for defining three or four clusters. The best performance index also proposed three and four clusters. Different dendrograms were created using centroid and Ward's methods to compare possible clusters.

Dendrograms built with the centroid method define two cluster positions on the left side of the graphic, which define one root node composed of basins ID13 to ID19 and ID23 to ID26 and another group with basins ID4 to ID12 and ID20 to ID22 (Figure 6A). Basins ID1 to ID3 are more distant and define a second root node. In these cases (Figure 6A,B), clustering responds primarily to basin area-related variables and secondary to the variables that represent parent rock composition (Figure 7A,B). Basins 1, 2, and 3 are the largest ones in the dataset. Basins 2 and 3 share a similar rock composition but differ significantly from Basin 1. Secondary parent rock composition defines the subgroups, but more dissimilarities still need to be a criterion for cluster definition. Cophenetic correlation of dendrograms Figure 6A,B are high with values of 0.80, but with the centroid method, higher values and outliers affect clustering.

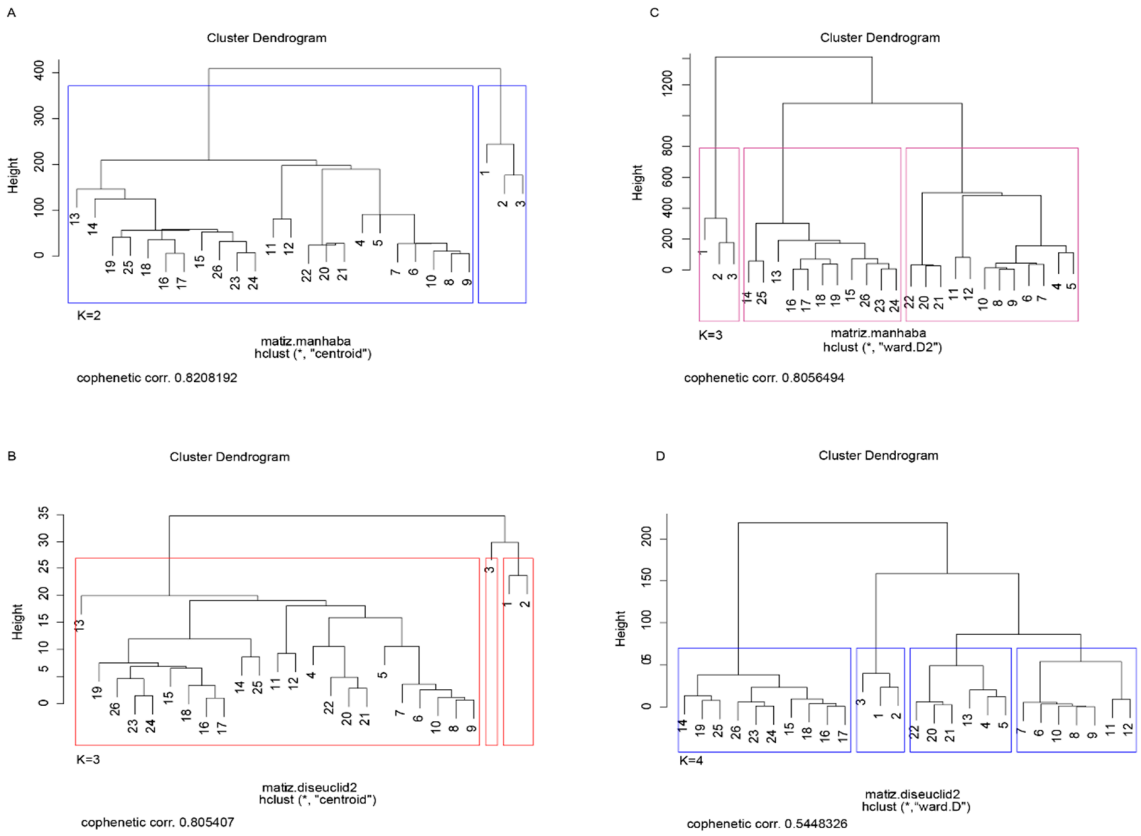

Figure 6. Dendrograms comparing different results according to centroid and Ward's methods. (**A**,**B**) are dendrograms obtained using Manhattan distance and Euclidean distance respectively, and the centroid method. (**C**,**D**) Dendrogram using Manhattan and Euclidean distances and the Ward methods'. Squares show clusters proposed for each method, according to each best performance index. Numbers labelled from 1 to 26 are basins IDs'.

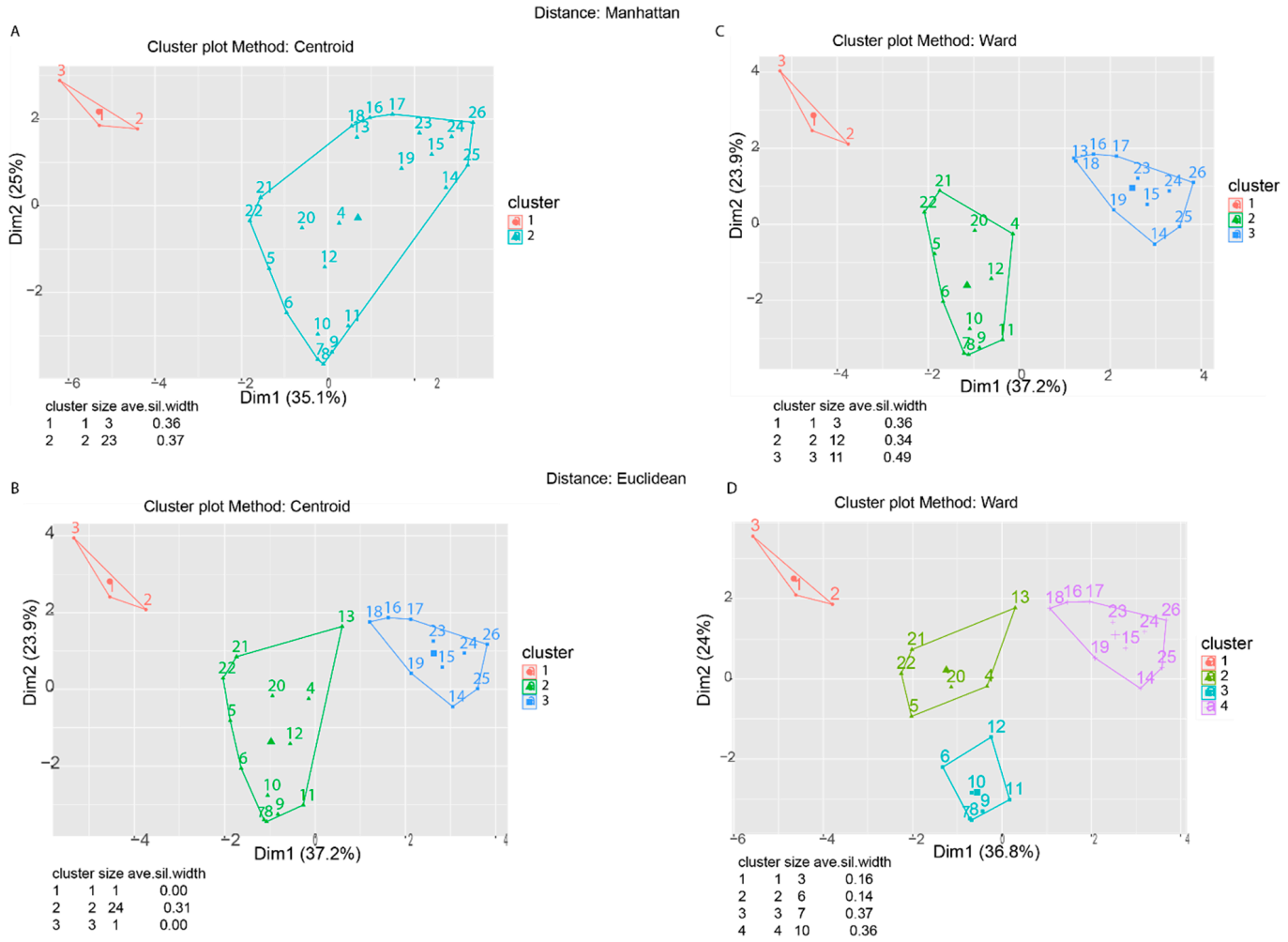

Figure 7. Clusters obtained using centroid and Ward methods obtained from correspondingly datasets of Figure 6. Numbers inside each cluster are basins IDs'. Clusters identified by colors and numbers. (**A**,**B**) are clusters obtained using Manhattan distance and Euclidean distance respectively, and the centroid method. (**C**,**D**) are clusters using Manhattan and Euclidean distances and the Ward methods'. Tables below each graphic indicated cluster ID, number of basins in each cluster and the average size width of each cluster.

Comparing the dendrograms obtained using the Ward method, clustering resulted in three and four clusters (Figures 6C,D and 7C,D), which respond better to substrate geological composition and morphometric characterization. Clustering performed with Manhattan distance gave a dendrogram with a high cophenetic correlation (0.8056). Like in the previous hierarchical clustering, group one includes Basins ID 1, 2, and 3 (Figures 7C and 8A,B). Cluster two includes igneous and high-grade metamorphic rocks basins (Figures 6C, 7C and 8A,B). Cluster three encompasses Basins ID13–19 and ID23–26, which substrate composition is sedimentary and medium-grade metamorphic rocks (Figures 6C, 7C and 8A,B). Clustering, defined by the Ward method and Euclidean distances, proposes four clusters but the cophenetic correlation is lower than the other dendrograms.

Outlining, the hierarchical clustering, defined by the Ward method using Manhattan distances, performs better in the morphometric and lithological-dependent variables (Table 5, Figures 6C, 7C and 8).

Table 5. Selected clustering using Manhattan distance and Ward's method.

Cluster	Basin ID	Ave.Width	Depare/Warea
1	1, 2, 3	0.36	0.148
2	4, 5, 6, 7, 8, 9, 10, 11, 12, 20, 21, 22	0.34	0.044
3	13, 14, 15, 16, 17, 18, 19, 23, 24, 25, 26	0.49	0.262

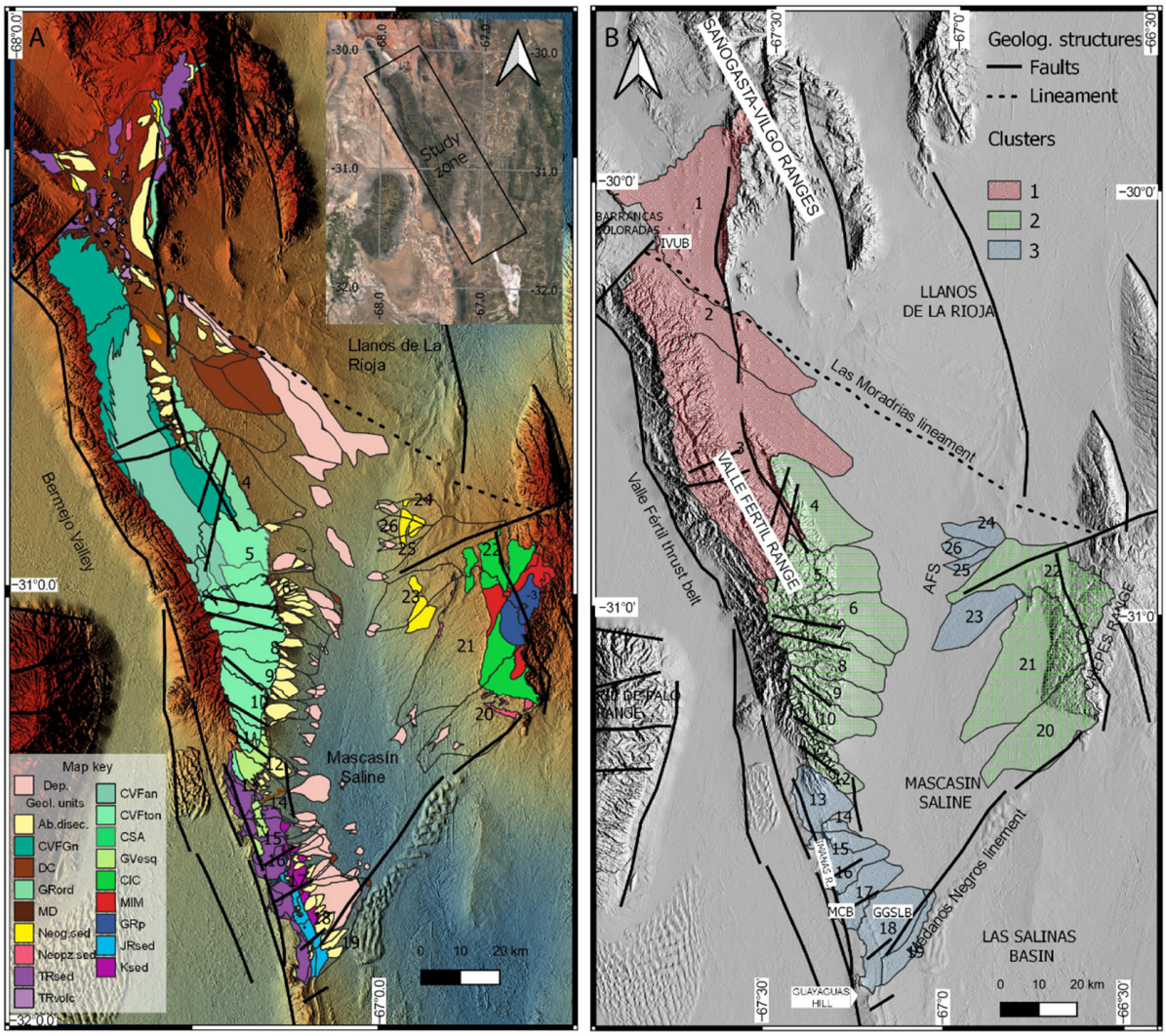

Figure 8. (**A**) Geological map showing stratigraphic units and main geological structures. (**B**) Map showing basin clustering. Numbers from 1 to 26 are drainage basins IDs'.

4.4. Depositional Areas

Digitalization of depositional areas shows different depositional products according to their location in the study area. Most of them develop in the transition unit and some of them reach the depression unit [32]. The depression unit opens from north to south, defining two large parts, one domain by the axial fluvial system (AFS) and the other by the Saline. In the northern part, the depression unit is highly restricted to the channel floor of the AFS, reaching almost 2.5 km width. The limited development of the depression unit is produced by an NW-SE structure (310° trend), developed in the transition unit, whose foothill is toward the SW (Figure 1). The NW-SE structure, named the Las Moradrias lineament in this work, divides the Salinas and Llanos de la Rioja valleys. Topographic profiles performed crossing the Mascasin Saline axis, from the western and eastern foothills

and the valley floor, allow us to observe changes in the piedmont slope and the depositional areas (Figures 1 and A4).

Profile number one has an SW-NE orientation, a length of 15 km with a slope of 0.46%, and develops at the foothills of the Valle Fértil mountain range (Figures A4 and 9). The central part of the profile presents a slightly convex morphology associated with fluvial deposits of the Las Moradrias and Punta del Médano Rivers (Basins ID1–2). The rivers of Basins ID1–2 display fluvial channels that produce elongated terminal lobes in a downstream direction with a restrictive distributary pattern (Figure 9A). A topographic high at the right end of profile one defines the northeastern limit between the Mascasin Saline Basin and the Llanos de La Rioja Watershed (Figures A2 and 9A). Profile two has a W-E orientation with a length of 50 km (Figure A2). This profile has an asymmetric morphology, and the western piedmont presents a concave shape while the eastern is convex. The western foothill is 19 km long with a slope of 0.98%, the eastern foothill is 31 km long with a slope of 0.84%, and the valley floor is 1 km wide. The main river of Basin ID3 displays fluvial channels that produce terminal lobes with a more noticeable distributary pattern than Basins ID1–2 (Figure 9B). In the eastern foothill, Basin ID22 reaches the AFS through fluvial bars in distributary channels, while Basins ID23–26 deposit isolated terminal lobes and fluvial bars.

Profile 3 has a W-E orientation with a length of 52 km and an asymmetric morphology (Figure A2). The western foothill has length of 20 km with a concave morphology and a slope of 1.68%. The eastern foothill is 32 km long with a convex morphology and a slope of 0.42%. The valley floor has a width of 2 km. From Basin ID4 to ID12, the higher slope of the transition unit produces depositional products as alluvial fans. These fans are downstream and restricted by a densely vegetated abandoned longitudinal dune field [22,77,78]. Depositional products of Basins ID20–21 are fluvial bars and terminal lobes displayed in the transition unit, covered by an abandoned longitudinal dune field that triggers fluvial deposition.

Toward the south, the transition unit slope reduces, and the valley floor (depression unit) is 7–8 km wide, reaching 12 km as the broadest extension of the Saline. Profile number four is located at the southern end of the Mascasín salt flat with a W-E orientation and has an extension of 51 km (Figure A4). The topographic profile shows a symmetrical morphology in which the western piedmont has a length of 22 km with a concave morphology and a slope of 0.65%. In contrast, the eastern piedmont has a convex morphology with a slope of 0.35%. The valley floor has a length of 8 km. From Basin ID13 to ID19, depositional products change to a distributive fluvial system in Basin ID13 and terminal lobes that reach the Saline. The transition units display smoother slopes, favoring DFS type systems development (0.9–1.4% [25]). An SW-NE structure borders the south part of the Mascasin Saline Basin, interpreted as an in-valley structural high [23,24]. Differing from the Valle Fértil range, the western piedmont of the Chepes range presents a more laterally extended transition unit occupied by an extended dunes field. These profiles show that the valley is asymmetrical, with a laterally extended eastern piedmont, a lower slope, and a convex morphology. The western piedmont has a greater slope and a concave morphology. The uplift of a series of hills with a meridian orientation generates the convex morphology of the eastern piedmont.

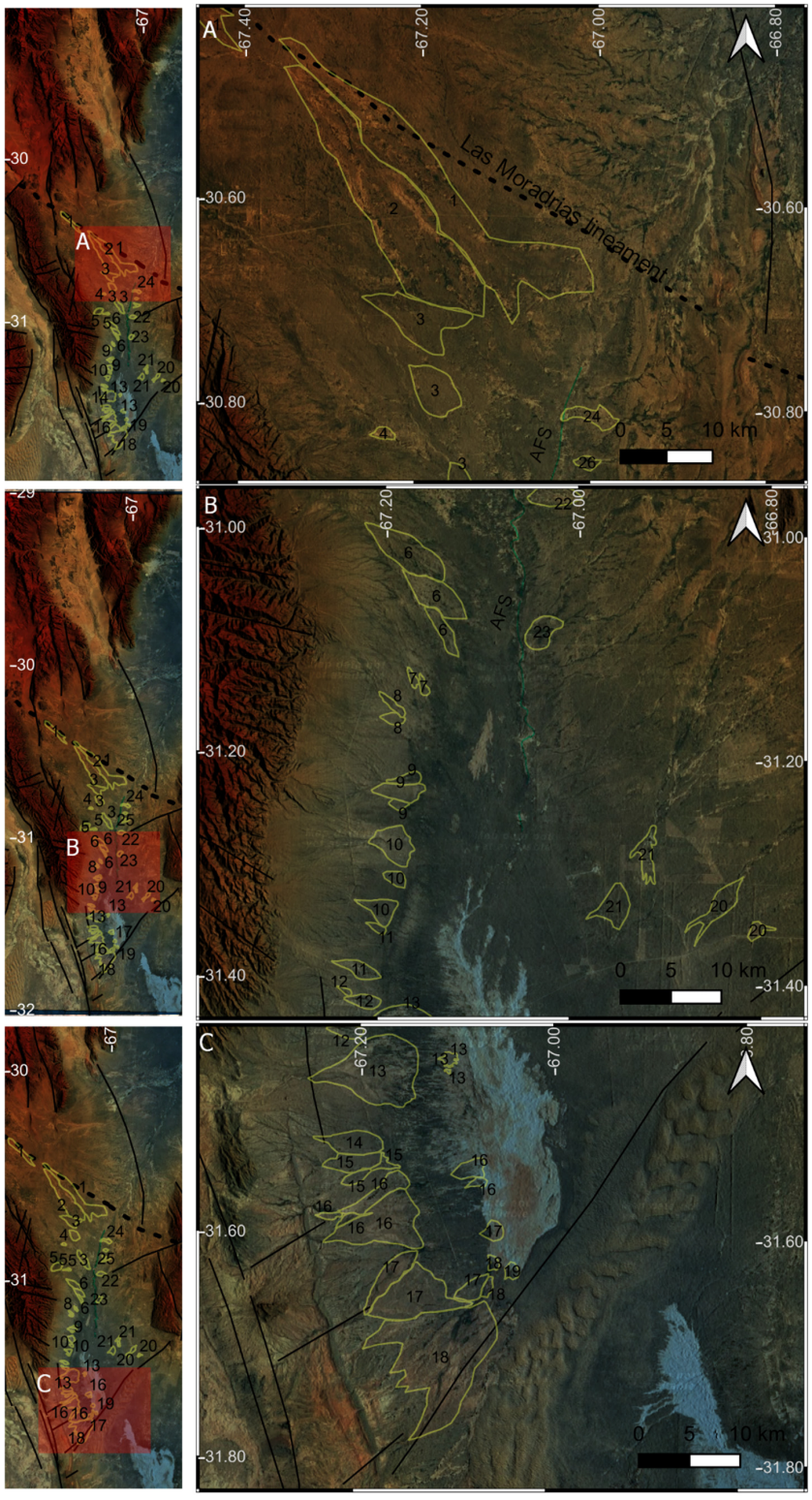

Figure 9. (**A**) Fluvial distributary and alluvial fans deposits of northwestern basins. (**B**) Alluvial fans and deposits of central part of Valle Fértil range. (**C**) Fluvial distributary deposits of southwestern part of Mascasin Saline Basin. Number from 1 to 26 refers to the feeder basins IDs' of the depositional landforms.

5. Discussion

The clustering of the morphometric and compositional variables shows between three and four major groups, and those are defined by the centroid method that displays a strong influence of the basin area variable outliers (Figures 6A and 7A). Clusters show that the lithological composition of the substrate is a decisive factor in the behavior of the variables.

The principal substrate composition in group three of the clusters (Figure 7B,C) and group four of cluster 7D are sedimentary rocks. Igneous rock defined another group, like group two of clusters 7B-C and groups three and four of clusters (Figure 7D). In all clusters, two of the three basins of group one have similar dominant substrates (metamorphic rocks, Basin 2 and 3). However, Basins ID1–3 are the largest ones, including Basin 3, considered an outlier (Table 4). Basin ID13 is the most challenging to gather since its position changes depending on the method used. For clusters generated from Manhattan distance, Basin ID13 is positioned closer to basins with predominantly sedimentary rocks and secondary metamorphic rocks. In contrast, in clusters generated by Euclidean distance, the position of Basin 13 is further away from its cluster, closer to group two.

Considering group homogeneity, clustering in 7C provides the best parameters (0.36 for group one, 0.34 for group two, and 0.49 for group three), high cophenetic correlation of 0.8056, and generating a fourth group does not necessarily improve homoscedasticity (Figures 7D and 8).

5.1. Parent Rock Composition and Clustering

Stratigraphy of the study zone shows three sedimentary basins positioned in the northwest and the southwest, which are the Ischigualasto-Villa Union Basin (IVUB), the Marayes-El Carrizal Basin (MCB), and the El Gigante Group of the San Luis Basin (GGSLB). The units that provide sediments from the IVUB are mostly the cemented sandstones and mudstones of the Talampaya, Tarjados, and Los Colorados formations and the basalts of the Cerro Morado [31,60,79–82]. Although these units produce resistant reliefs, their competence is much lower than that of the metamorphic rocks in the northern part of the Valle Fértil range (CVFGn and CVFan). Basin relief displays higher values toward the metamorphic and igneous rocks of the Valle Fertil–La Huerta and Chepes ranges, becoming maximum in the igneous geological units (CVFton). A similar scenario occurs in the southern part of the study zone where argillaceous mudstones of the Carrizal and Quebrada del Barro formations (MCB [29]) form depressions, while conglomerates and sandstones of the Quebrada del Puma, Balde de Leyes, and Rancho Grande formations (MCB, [27]), and the conglomerates of the Toscal and La Cruz formations (GGSLB, [83]) contour resistant reliefs. Correspondingly, morphometric parameters sensitive to physical weathering, such as basin relief, relief factor, and Melton ruggedness index, correlate with changing rock compositions. Basin morphology indexes do not show a straightforward correlation with lithology; they do respond to geological structures (Figure 8). The orientation of dominant structures coincides with the elongation axis of the basins. The NW trend of main structures like the Valle Fértil thrust belt controls Basins 1 and 2. The WNW-ESE structures of the igneous core of the Valle Fértil–La Huerta ranges [30] define Basins 5 to 13, while Mesozoic WSW-ENE structures control Basins 14 to 19 [23,24]. In the Chepes range, combined NW and NE structures govern basin morphological parameters.

Two main factors play a critical role in clustering besides basin area: parent rock composition, which controls basin relief, relief factor, Melton ruggedness index, and drainage density; and tectonic control, which strongly influences morphometric parameters through the elongation ratio, form factor, circularity index, and compactness coefficient, and the drainage orientation.

In this study, under similar climatic conditions (semi-arid to arid), different reliefs are observed to be produced by lithological composition. Higher drainage density, lower basin reliefs, and height reveal the easily eroded sedimentary rock substrate compared to those parameters observed where igneous rocks are. Igneous rocks form lower drainage density, higher basin reliefs, and height, revealing their resistant competence to physical weathering. As is expected, metamorphic rocks present intermediate reliefs between igneous and sedimentary rocks. Metamorphic rocks exert greater control over basin shape than igneous and sedimentary rocks. According to the results, decreasing values of the circularity ratio appear when metamorphic rocks outcrop, possibly related to the structural foliation inherited from its complex geological evolution.

Climatic imprints on basin evolution could be hidden by the short temporal range of the variable used in this study [48]. However, the geological record during the Pliocene and Quaternary, from when the ranges started exhumation, suggested that the climate in the region was quite similar to the present one [22,38]. Many authors interpreted that semi-arid and arid conditions could explain slow exhumation rates despite the active tectonics and vertical uplift that characterized the region [22,37,38]. This scenario highlights parent rock composition as a critical control in landscape modeling. For the Mascasin Saline Basin, rock composition and tectonically driven forces were the primary factors that modeled basin morphology, and controlled drainage orientation. Depositional products are primary controlled by basin morphology, but especially for compositionally dependent parameters related to slope (Figure 10). Landscapes derived by climatic control such as an eolian dunes field affect depositional products facies architecture since the dunes field trigger avulsion and upstream aggradation of fluvial channels [1,84].

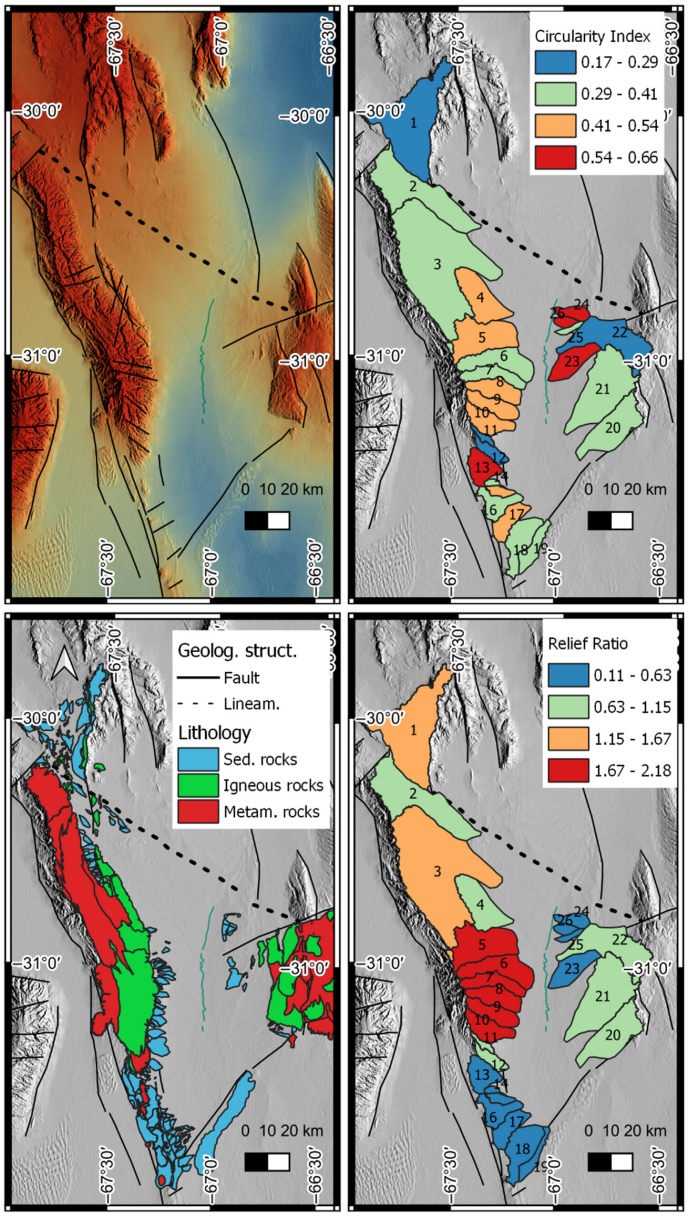

Figure 10. Maps showing primary factors that controlled basin drainage morphology, those related to tectonics and those related to lithological composition. Lithology is grouped into the three main groups: Sed. rocks (sedimentary rocks), Igneous rocks, Metam. rock (metamorphic rocks). Numbers labelled from 1 to 26 are basins IDs'.

A stronger influence of climate on watershed morphometry would be determined in basins where feeder drainage systems develop under extreme differences in climate types [2].

5.2. Parameters That Influence Depositional Areas

The Dep.area variable is positive and moderately correlated with watershed areas, representing between 5 and 30% of the feeder drainage basin area (Table 5). Depositional areas from cluster one (sedimentary, volcanic, and foliated metamorphic rocks) represented almost 15% of the basin area. In cluster two, represented mainly by igneous parent rocks and secondary by weakly foliated metamorphic rocks, the derived depositional bodies have a mean area representing only 4% of the basin area (Table 5). Sedimentary and foliated metamorphic parent rocks (cluster three) produce a greater proportion of the depositional area, 26% of the basin area. Depositional areas tend to be larger in basins with more weatherable rock outcrops. Therefore, this is not related to higher drainage density, which negatively correlates with depositional areas; it seems to depend on other factors, such as the shape of the basin and the smoother slopes that favor channelization after loose confinement and downstream sheet flood occurrence [26,85–87]. For example, sedimentary and metamorphic rocks favor smother slopes in the transition unit from the Papagayos Creek (Basin ID13) to the Guayaguas River (Basin ID19). Channelized flows and fluvial deposits occur once loose confinement occurs, allowing sediments to reach broader areas at the depression unit. In comparison, in the Valle Fértil range, mainly composed of igneous rocks, the restricted widening of the transition unit and its high slope produces non-channelized flows, once loose confinement occurs, limiting the downstream aggradation over the depression unit.

In conclusion, the basin area and the parent rock composition control depositional products. The role of climate on depositional products remains unsolved due to climatic conditions in the study zone. However, larger depositional areas display a weak to moderate correlation with watersheds characterized by lower precipitations (−0.38 value of the Spearman correlation coefficient).

In the Saline Mascasin Basin, the orientation of depositional areas deposited by transversal drainage systems presents a strong structural control, which differs from that of other intermontane valleys, like the North Bermejo Valley. The Huaco DFS transversal drainage system enters the Bermejo Valley in a W-E direction and turns parallel to the regional drainage outlet in an SE direction [87,88]. Like the Bermejo Valley, the Las Salinas Basin has a regional drainage outlet to the SE. However, the Mascasin Saline is limited by a set of structures that form a triangular shape endorheic depocenter limited by NW-SE (330°), WNW-ENE (300°), and NE-SW (40°) faults. These fault systems exert strong control over depositional products, avoiding their alignment with the AFS that follows the regional drainage orientation. This situation occurs even in the south part of the Mascasin Saline, where the transition unit presents low slope and high aggrading fluvial systems like the Papagayos DFS, although smaller in size than the Huaco DFS [28,88].

5.3. Role of Morphometric Parameters in Papagayos DFS Occurrence

The Papagayos River produces a fan shaped depositional area that stands out when observing the Mascasin Saline Basin from an aerial view. The Papagayos River's sedimentary environment develops a downstream facies architecture where fluvial deposits show the downstream loss of capacity and competence of channels, interpreted as a distributive fluvial system [28]. Crevasse and terminal lobes accretion are the main sedimentary processes in floodplain deposition in the Papagayos DFS, composed of muddy facies that provide the convex fan morphology over the transition unit.

Comparing the morphometric parameters of the Papagayos Basin with those of the other basins of cluster three, we see that they share similar conditions, though only the Papagayos displays this high aggrading fluvial system. The basins of cluster three are developed in

sedimentary and metamorphic rocks, and have a low slope, dominant arid conditions, high drainage density, and smaller sizes compared to the other clusters. However, the Papagayos Basin's shape parameters differ from those of its group. Congruently, structural control of the Papagayos Basin is different, since a W-E lineament controls it outlet and profuse neotectonics with an NW-SE trend limits the margin of the basin [26]. The shape parameters of the Papagayos Basin reveals that it stands out for its round to oval morphology, which is reported for its high values of form factor, elongation ratio, and circularity index and low values of compactness coefficient. Thus, the particular shape of the Papagayos Basin and the high structural control drainage favor high peak discharges and promotes flow potency [56,57,59]. A combination of low reliefs and low slope parameters, high drainage density, well-organized drainage, and oval-shaped morphology gives a perfect recipe for producing channels with enough capacity and competence to transport and organize sediment towards the depocenter forming a high aggrading distributive fluvial system.

6. Conclusions

The Mascasin Saline displays a triangular-shaped depocenter limited by three faults where a local drainage organization prevails. The geological structures that limit the triangle-shaped depocenter are the NW trend Valle Fertil thrust belt [26,30,32,33], the NE trend faults of the Medanos Negros [23,24], and the Las Moradrias lineament NW-SE.

Different approaches allow for unraveling the main controls on drainage systems and depositional products of the Mascasin Saline Basin. Clustering analysis helps in understanding the relation between morphometric parameters and parent rock composition. The control exerted by the semi-arid climate that characterizes the region presents no significant relation with morphometric parameters. Therefore, different reliefs and landscapes are produced by combining two main factors: watershed parent rock composition and tectonic structures.

Parent rock composition controls basin relief and slope-related parameters. High slope and relief basins comprise igneous rocks, and lower slopes and relief basins are those where sedimentary rocks dominate. Also, the drainage density of a basin of a similar area is sensitive to parent rocks beside the basin area, showing the highest values for sedimentary parent rocks (values above 4). In contrast, igneous and metamorphic rocks mostly show high to low values (up to 3). Shape parameters exhibit more relation with tectonic structures. Watersheds are elongated following different structure systems of the study zone, not only the major structures of the NW-SE trend but also oblique structures. Metamorphic rocks also produce basins with a higher trend toward circular morphologies.

The combination of both factors produces different depositional products. Climate shows a negative weak correlation with depositional areas, interpreted as under lower precipitation; the depositional areas are larger and vice versa, as proposed before in the literature [2,14]. In the study zone, the transition unit displays high to low slopes according to rock composition in the watersheds. The depositional products of higher piedmont slopes, related to igneous parent rock composition, are alluvial fan types with restricted downstream accretion. While depositional products of sedimentary parent rock composition, developed in low piedmont slopes, are fluvial distributary deposits. Basin area is a primary control over depositional areas, though basins of similar sizes developed over sedimentary rocks turn to produce larger depositional areas than those developed over igneous rocks. Another critical control over depositional areas is geological structures, which define the orientation of main rivers that feed depositional bodies despite the regional drainage outlet.

Despite there are many basins comprise sedimentary parent rocks, but only the Papagayos Basin produces a manifest convex fan-shaped morphology deposit. The downstream succession of sedimentary environments exhibiting the decreasing capacity and competence of the channels allows for defining the Papagayos DFS. Differing from the other

basins that share the same cluster, the Papagayos Basin tends to display a circular/rounded shape. A basin with tendecy to circular morphology produces a more efficient transport of sediments and flows out of the basin; according to our results, this aspect is considered a critical condition promoting DFS formation.

Supplementary Materials: The R script to perfom the hierchichal clustering (Geomatics_SantiMalnis& Rothis.r file) is available at https://drive.google.com/file/d/1HNzu-nKf6EfB4u536mYh8ZqxojO6ocEm/view?usp=drive_link (accessed on 23 December 2024).

Author Contributions: Conceptualization, P.S.M.; methodology, P.S.M. and L.M.R.; software, P.S.M. and L.M.R.; formal analysis, P.S.M.; investigation, P.S.M. and L.M.R.; resources, L.M.R.; writing—original draft preparation, P.S.M. and L.M.R.; writing—review and editing, P.S.M. and L.M.R.; visualization, P.S.M. and L.M.R. All authors have read and agreed to the published version of the manuscript.

Funding: This research was funded by PICT 2019 04160 FONCYT, PROJOVI-UNSJ 101202103000056SJ-2021-2022.

Data Availability Statement: R script is in the Supplementary Materials. https://drive.google.com/file/d/1HNzu-nKf6EfB4u536mYh8ZqxojO6ocEm/view?usp=drive_link (accessed on 23 December 2024).

Conflicts of Interest: The authors declare no conflict of interest.

Appendix A

Appendix A.1. Drainage Basins (Section 4.1)

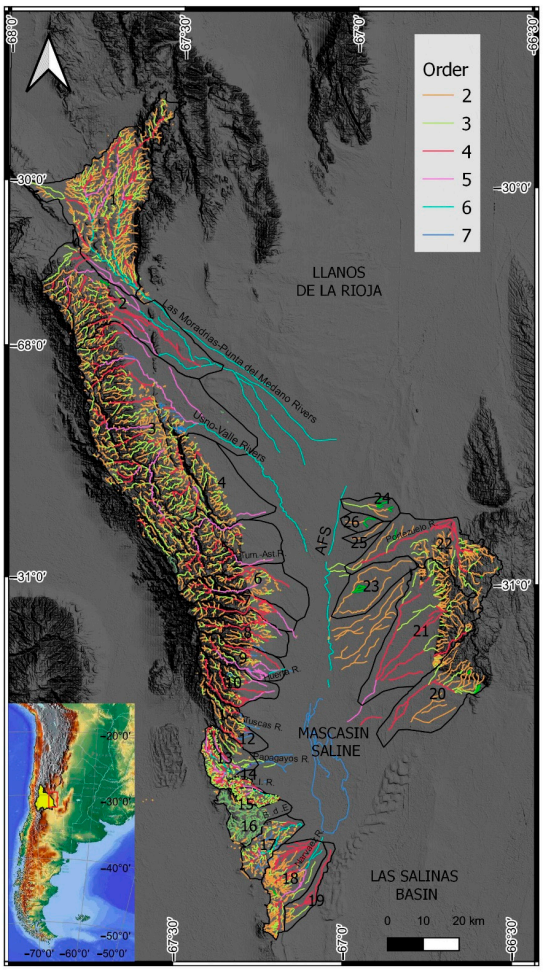

Figure A1. Drainage basins of Mascasin Saline. Channels labeled from Strahler order 2. Tum.-Ast. R.: Las Tumanas-Astica Rivers; L.I.R.: Las Imanas River; B.d.E. R.: Bajos del Estanque River. Numbers labelled from 1 to 26 ar basins IDs'.

Appendix A.2. Exploratory Data Analysis (Section 4.3)

Table A1. Exploratory data analysis.

Variable	Mean	sd	*n*
Area_cca	293.00	334.24	26
Perim_cca	90.92	61.08	26
Clima	298.69	68.46	26
Hr	0.8484615	0.70059799	26
Dd	6.079	7.125	26
%IG	40.23	43.11	26
%Met	15.84	24.16	26
%RSED	38.88	45.42	26
Deparea	33.83	51.04	26
L (km)	28.65	13.59	26
Kc	1.633	0.31554105	26
C	0.4026923	0.12919931	26
E	0.5842308	0.09617372	26
Ff	0.2753846	0.09326224	26
Rr	0.0300000	0.02280351	26

Histograms and Boxplot

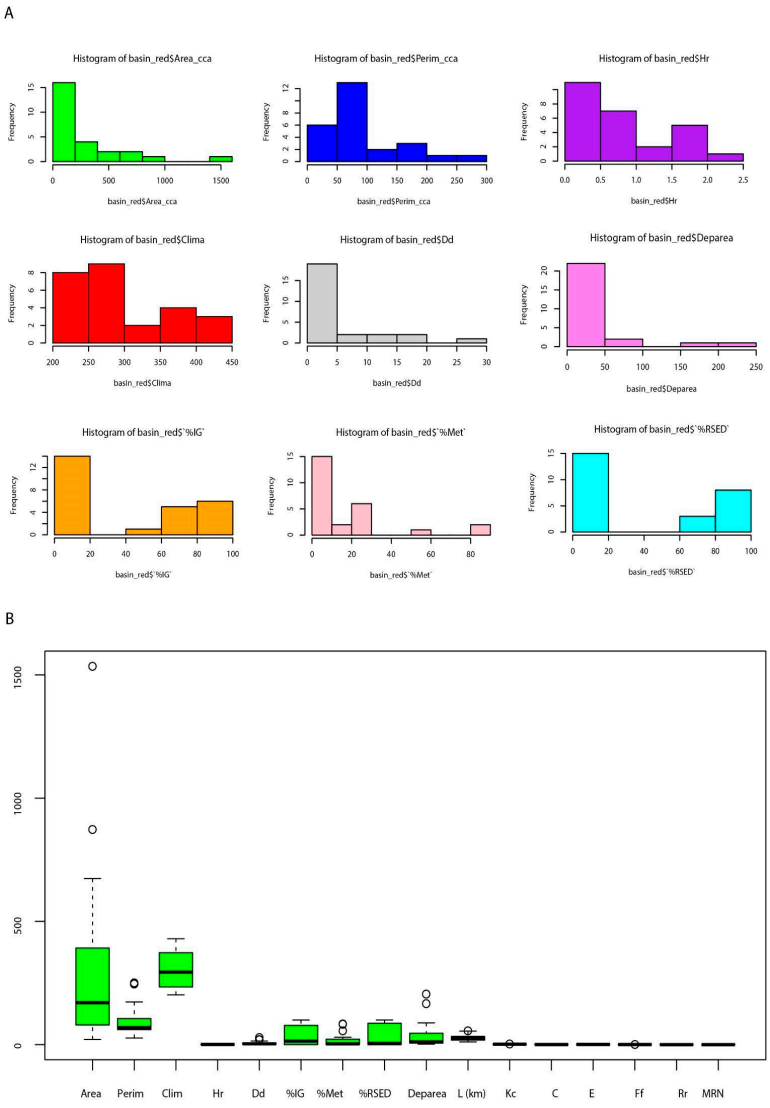

Figure A2. Exploratory analysis of data. (**A**) Histogram of some variables pursued to visually inspect possible normal behavior. (**B**) Boxplot of all variables looking for outliers. Variables labeled as: Hr:

basin relief; Perim_cca: basin perimeter; L (km): basin length. Area_cca: basin area; %IG: parent rocks of igneous dominant lithology; Rr: relief factor; MRN: Melton ruggedness number; Kc: compactness coefficient; %Met: parent rocks of metamorphic dominant lithology; Deparea: area of active depositional products of each river; Ff: form factor; E: elongation ratio; Clima: mean annual precipitation; C: circularity ratio; %RSED: parent rocks of sedimentary dominant lithology; Dd: drainage density.

Appendix A.3. Dataset Used in the Hierchical Clutsering (Section 4.4)

ID	Area (km2)	Perim (km)	L (km)	Clima (mm)	Hr	Dd	Kc	C	E	Ff	Rr	MRN	Deparea	%IG	%Met	%RSED
1	873	251	56	201.75	1.42	0.68	2.38	0.17	0.6	0.28	0.03	0.05	204.94	16	0	84
2	674	169	56	228.66	0.95	0.89	1.82	0.3	0.52	0.21	0.02	0.04	166.54	9	83	8
3	1535	246	55	251.33	1.23	0.39	1.76	0.32	0.8	0.51	0.02	0.03	84.59	12	84	0
4	322	89	32	318	0.73	1.86	1.39	0.51	0.63	0.31	0.02	0.04	2.47	100	0	0
5	406	106	31	318	1.94	1.47	1.47	0.45	0.73	0.42	0.06	0.1	22.95	70	30	0
6	288	97	33	296	1.91	2.08	1.6	0.38	0.58	0.26	0.06	0.11	40.59	93	7	0
7	158	77	30	296	1.84	3.78	1.72	0.33	0.47	0.18	0.06	0.15	2.37	99	1	0
8	185	69	26	296	2.18	3.23	1.42	0.49	0.59	0.27	0.08	0.16	4.05	100	0	0
9	163	66	26	296	1.92	3.67	1.45	0.47	0.55	0.24	0.07	0.15	11.00	100	0	0
10	177	72	26	252.3	1.78	3.38	1.52	0.43	0.58	0.26	0.07	0.13	19.11	96	4	0
11	31	48	14	234	0.72	19.28	2.41	0.17	0.45	0.16	0.05	0.13	5.97	78	22	0
12	80	63	20	234	0.77	7.47	1.97	0.25	0.5	0.2	0.04	0.09	4.14	44	56	0
13	163	61	18	234	0.37	3.67	1.34	0.55	0.8	0.5	0.02	0.03	47.82	0	0	0
14	21	27	11	232	0.21	28.46	1.65	0.36	0.47	0.17	0.02	0.05	10.75	0	27	73
15	46	33	13	232	0.24	12.99	1.36	0.53	0.59	0.27	0.02	0.03	8.29	0	22	78
16	148	68	21	232	0.14	4.04	1.57	0.4	0.65	0.34	0.01	0.01	48.26	0	13	87
17	147	62	21	256	0.15	4.07	1.43	0.48	0.65	0.33	0.01	0.01	46.80	0	1	99
18	224	87	29	292	0.33	2.67	1.63	0.37	0.58	0.27	0.01	0.02	88.51	0	2	98
19	125	64	28	292	0.2	4.78	1.6	0.38	0.45	0.16	0.01	0.02	1.77	0	0	100
20	392	117	40	412	0.96	1.52	1.65	0.36	0.56	0.25	0.02	0.05	11.18	75	18	7
21	641	156	45	429.5	0.73	0.93	1.73	0.33	0.64	0.32	0.02	0.03	15.52	77	21	2
22	476	173	44	419.5	0.72	1.26	2.22	0.2	0.56	0.25	0.02	0.03	8.52	77	21	2
23	197	64	28	373	0.23	3.03	1.28	0.6	0.57	0.25	0.01	0.02	7.79	0	0	100
24	75	40	17	380	0.16	7.97	1.29	0.59	0.57	0.26	0.01	0.02	8.35	0	0	100
25	30	31	14	380	0.12	19.92	1.58	0.39	0.44	0.15	0.01	0.02	6.37	0	0	100
26	41	28	11	380	0.11	14.58	1.22	0.66	0.66	0.34	0.01	0.02	2.81	0	0	100

Figure A3. Dataset under study. Variables labeled as: Area: basin area; Perim_cca: basin perimeter; L (km): basin length; Clima: mean annual precipitation; Hr: basin relief; Dd: drainage density; Kc: compactness coefficient; C: circularity ratio; E: elongation ratio; Ff: form factor; Rr: relief factor; MRN: Melton ruggedness number; Deparea: area of active depositional products of each basin main river; %IG: parent rocks of igneous dominant lithology, %Met: parent rocks of metamorphic dominant lithology; %RSED: parent rocks of sedimentary dominant lithology.

Appendix A.4. Topographic Profles

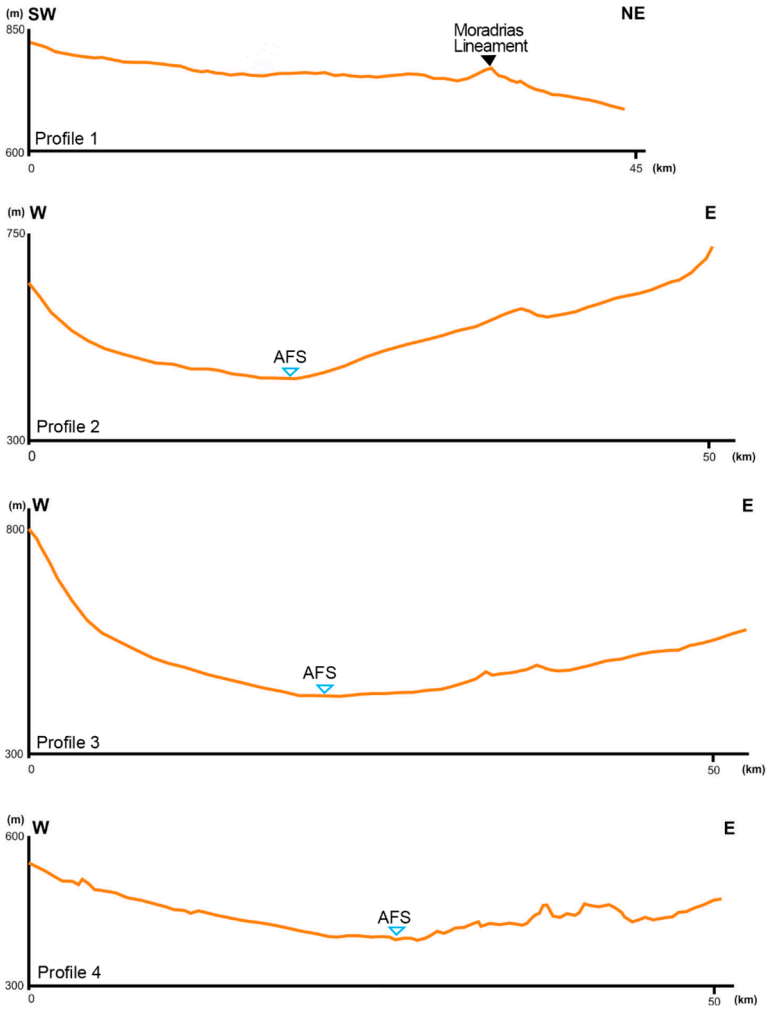

Figure A4. Topographic profiles in transition and depression units of Mascasín Saline Basin. Geographic locations of profiles in Figure 1.

References

1. Blair, T.; Mcpherson, J. Alluvial fans and their natural distinction from rivers based on morphology, hydraulic processes, sedimentary processes, and facies assemblages. *J. Sediment. Res.* **1994**, *A64*, 450–489.
2. Tucker, G.E.; Slingerland, R. Drainage basin responses to climate change. *Water Resour. Res.* **1997**, *33*, 2031–2047. [CrossRef]
3. Le Pera, E.; Arribas, J.; Critelli, S.; Tortosa, A. The effects of source rocks and chemical weathering on the petrogenesis of siliciclastic sand from the Neto River (Calabria, Italy): Implications for provenance studies. *Sedimentology* **2001**, *48*, 357–378. [CrossRef]
4. Thorpe, M.T.; Hurowitz, J.A. Unraveling sedimentary processes in fluvial sediments from two basalt dominated watersheds in northern Idaho, USA. *Chem. Geol.* **2020**, *550*, 119673. [CrossRef]
5. Marchi, L.; Dalla Fontana, G. GIS morphometric indicators for the analysis of sediment dynamics in mountain basins. *Environ. Geol.* **2020**, *48*, 218–228. [CrossRef]
6. Melton, M.A. *An Analysis of the Relations Among Elements of Climate, Surface Properties, and Geomorphology*; Columbia Univ.: New York, NY, USA, 1957; pp. 1–99.
7. Melton, M.A. The geomorphic and paleoclimatic significance of alluvial deposits in southern Arizona. *J. Geol.* **1965**, *73*, 1–38. [CrossRef]
8. Viaplana-Muzas, M.; Babault, J.; Dominguez, S.; Van Den Driessche, J.; Legrand, X. Drainage network evolution and patterns of sedimentation in an experimental wedge. *Tectonophysics* **2015**, *664*, 109–124. [CrossRef]
9. Dickinson, W.R.; Suczek, C.A. Plate tectonics and sandstone compositions. *Aapg Bull.* **1979**, *63*, 2164–2182.
10. Dickinson, W.R. Provenance and sediment dispersal in relation to paleotectonics and paleogeography of sedimentary basins. In *New Perspectives in Basin Analysis*; Springer: New York, NY, USA, 1988; pp. 3–25. [CrossRef]

11. Tooth, S.; Nanson, G.C. Anabranching rivers on the Northern Plains of arid central Australia. *Geomorphology* **1999**, *29*, 211–233. [CrossRef]
12. Weltie, G.J.; Von Eynatten, H. Quantitative provenance analysis of sediments: Review and outlook. *Sediment. Geol.* **2004**, *171*, 1–11. [CrossRef]
13. Jain, M.; Tandon, S.K. Quaternary alluvial stratigraphy and palaeoclimatic reconstruction at the Thar margin. *Curr. Sci.* **2003**, *84*, 1048–1055.
14. Tucker, G.E.; Bras, R.L. Hillslope processes, drainage density, and landscape morphology. *Water Resour. Res.* **1998**, *34*, 2751–2764. [CrossRef]
15. Schumm, S.; Hadley, R. *Progress in the Application of Landform Analysis in Studies of Semiarid Erosion*; US Department of the Interior Geological Survey Circular: Washington, DC, USA, 1961; Volume 437, pp. 1–14.
16. Bookhagen, B.; Strecker, M.R. Spatiotemporal trends in erosion rates across a pronounced rainfall gradient: Examples from the southern Central Andes. *Earth Planet. Sci. Lett.* **2012**, *327*, 97–110. [CrossRef]
17. Tucker, G.E.; Hancock, G.R. Modelling landscape evolution. *Earth Surf. Process. Landf.* **2010**, *35*, 28–50. [CrossRef]
18. Migoń, P.; Duszyński, F. Landscapes and landforms in coarse clastic sedimentary tablelands–is there a unifying theme? *Catena* **2022**, *218*, 106545. [CrossRef]
19. Yunus, A.P.; Oguchi, T.; Hayakawa, Y.S. Morphometric Analysis of Drainage Basins in the Western Arabian Peninsula Using Multivariate Statistics. *Int. J. Geosci.* **2014**, *5*, 527–539. [CrossRef]
20. Suvires, G. Geomorfología de la Provincia de San Juan. In *Catálogo de Recursos Humanos e Información Relacionada con la Temática Ambiental en la Región Andina Argentina*; Abraham, M.E., Rodríguez Martínez, F., Eds.; C-Bra Systematics GTZ: Buenos Aires, Argentina, 1996; Chapter 11. Available online: https://www.mendoza-conicet.gob.ar/ladyot/catalogo/cdandes/cap11.htm (accessed on 20 June 2017).
21. Criado Roque, P.; Mombrú, C.A.; Ramos, V. Estructura e interpretación tectónica. In *Geología y Recursos Naturales de la Provincia de San Luis, Proceedings of the VIII Congreso Geológico Argentino, San Luis, Argentina, 20–26 September 1981*; Relatorio, Irigoyen, M., Eds.; 1981; pp. 155–192. Available online: https://www.researchgate.net/publication/284295627_Estructura_e_interpretacion_tectonica_en_Geologia_y_Recursos_Naturales_de_la_Provincia_de_San_Luis (accessed on 23 December 2024).
22. Tripaldi, A.; Forman, S.L. Geomorphology and chronology of Late Quaternary dune fields of western Argentina. *Palaeogeogr. Palaeoclimatol. Palaeoecol.* **2007**, *251*, 300–320. [CrossRef]
23. Azeglio, E.A.; Giménez, M.E.; Introcaso, A. Análisis de subsidencia de la Cuenca de las Salinas, Sierras Pampeanas occidentales. *Rev. Asoc. Geológica Argent.* **2008**, *63*, 272–280.
24. Azeglio, E.A.; Gimenez, M.E.; Introcaso, A. Interpretation of Las Salinas sedimentary basin-Argentina, based on integration of geological and geophysical data. *Geofísica Int.* **2010**, *49*, 225–244. [CrossRef]
25. Santi Malnis, P.; Colombi, C.E.; Rodríguez Posatini, N.; Rothis, L.M.; Limarino, C.O. Caracterización sedimentológica de un Sistema Fluvial Distributivo de clima árido: Arroyo Papagayos, en el piedemonte oriental de las Sierras La Huerta-Imanas, San Juan, Argentina. *Andean Geol.* **2018**, *45*, 186–228. [CrossRef]
26. Suriano, J.; Limarino, C.O. Sedimentación pedemontana en las nacientes del Río Jáchal y Pampa de Gualilán, Precordillera de San Juan. *Rev. Asoc. Geológica Argent.* **2009**, *65*, 516–532.
27. Colombi, C.E.; Santi Malnis, P.; Martínez, R.N.; Drovandi, J.M.; Correa, G.A.; Soria Pures, T.B. Revisión estratigráfica y evolución paleoambiental del mesozoico temprano al sureste de la provincia de San Juan, Argentina. *Rev. Asoc. Geológica Argent.* **2021**, *784*, 449–486.
28. Jordan, T.; Isacks, B.; Allmendinger, R.W.; Brewe, J.A.; Ramos, V.A.; Ando, C.J. Andean tectonics related to geometry of subducted Nazca plate. *GSA Bull.* **1983**, *94*, 341–361. [CrossRef]
29. Bossi, G. Geología de la Cuenca de Marayes-El Carrizal (Provincia de San Juan), República Argentina. In Proceedings of the Actas del VI Congreso Geológico Argentino, I, Bahia Blanca, Argentina, 21–27 September 1976; pp. 23–38.
30. Vujovich, G.; Chernicoff, C.; Tchilinguirian, P.; Godeas, M.; Marín, G.; Pezzutti, N.; Diaz, I. Hoja Geológica 3166-III. Chepes, provincias de La Rioja, San Juan y San Luis, Buenos Aires. *Bol. Serv. Geol. Argent.* **2007**, *251*, 1–65.
31. Net, L.; Limarino, O. Paleogeografía y correlación estratigráfica del Paleozoico Tardío de la Sierra de Los Llanos, provincia de La Rioja, Argentina. *Rev. Asoc. Geológica Argent.* **1999**, *54*, 229–239.
32. Rothis, L.M.; Haro, F.M.; Perucca, L.P.; Santi Malnis, P.; Alcacer, J.M.; Vargas, N. *Morphotectonic Analysis in the Eastern Piedmont of the Sierra de La Huerta, Western Sierras Pampeanas, San Juan, Argentina*; Advances in Geomorphology and Quaternary Studies in Argentina: Special Symposium from the Argentine Association of Geomorphology and Quaternary Studies; Springer International Publishing: Cham, Switzerland, 2020; pp. 114–128. [CrossRef]
33. Bastías, H.; Uliarte, E.; Paredes, J.; Sanchez, A.; Bastías, J.; Ruzycki, L.; Perucca, L. Neotectónica de la provincia de San Juan. In *11º Congreso Geológico Argentino*; Bordonaro, O., Ed.; Relatorio de Geología y Recursos Naturales de la Provincia de San Juan: San Juan, Argentina, 1990; pp. 228–245.

34. Rothis, L.M.; Perucca, L.P.; Santi Malnis, P.; Alcacer, J.M.; Haro, F.M.; Vargas, H.N. Neotectonic, morphotectonic and paleoseismologic analysis of the Las Chacras Fault System, Sierras Pampeanas Occidentales, San Juan, Argentina. *J. S. Am. Earth Sci.* **2019**, *91*, 144–153. [CrossRef]
35. Rothis, L.M. Análisis de la Actividad Tectónica Cuaternaria en el Sector sur de la Falla Las Chacras y Evaluación de la Peligrosidad Sísmica. Sierras Pampeanas Occidentales. Provincia de San Juan. Doctoral Thesis, National University of San Juan, San Juan, Argentina, 2016.
36. Costa, C.H.; Gardini, C.E.; Ortíz Suárez, A.E.; Chiesa, J.O.; Ojeda, G.E.; Rivarola, D.L.; Strasser, E.; Morla, P.; Ulaco, J.; Tornelli, G.; et al. *Hoja Geológica 3366-I San Francisco del Monte de Oro*; Instituto de Geologia y Recursos Minerales, Servicio Geológico Minero Argentino Boletin: Buenos Aires, Argentina, 2001; 278p.
37. Löbens, S.; Bense, F.A.; Dunkl, I.; Wemmer, K.; Kley, J.; Siegesmund, S. Thermochronological constraints of the exhumation and uplift of the Sierra de Pie de Palo, NW Argentina. *J. S. Am. Earth Sci.* **2013**, *48*, 209–219. [CrossRef]
38. Bense, F.; Costa, C.; Oriolo, S.; Löbens, S.; Dunkl, I.; Wemmer, K.; Siegesmund, S. Exhumation history and landscape evolution of the Sierra de San Luis (Sierras Pampeanas, Argentina)-new insights from low-temperature thermochronological data. *Andean Geol.* **2017**, *44*, 275. [CrossRef]
39. Ezpeleta, M.; Dávila, F.M.; Astini, R.A. Estratigrafía y paleoambientes de la Formación Los Llanos (La Rioja): Una secuencia condensada miocena en el antepaís fragmentado andino central. *Rev. Asoc. Geológica Argent.* **2006**, *61*, 171–186.
40. Cioccale, M.A. Climatic fluctuations in the Central Region of Argentina in the last 1000 years. *Quat. Int.* **1999**, *62*, 35–47. [CrossRef]
41. Garzanti, E.; Capaldi, T.; Tripaldi, A.; Zárate, M.; Limonta, M.; Vezzoli, G. Andean retroarc-basin dune fields and Pampean Sand Sea (Argentina): Provenance and drainage changes driven by tectonics and climate. *Earth-Sci. Rev.* **2022**, *231*, 104077. [CrossRef]
42. Sitio del Servicio Meteorológico Nacional Argentino. 2020. Available online: https://www.smn.gob.ar/clima/vigilancia (accessed on 29 October 2024).
43. INTA Digital Geo. 2023. Available online: https://geo.inta.gob.ar/es#7.1/-30.623/-67.604 (accessed on 29 October 2024).
44. Karlin, M. Cambios temporales del clima en la subregión del Chaco Árido. *Multequina* **2012**, *21*, 3–16.
45. Pereyra, B. Clima de la provincia de San Juan. In *Catálogo de Recursos Humanos e Información Relacionada con la Tematica Ambiental en la Region Andina Argentina*; Online (2000) C-Bra Systematics; GTZ en el marco de la Cooperación Técnica Argentino-Alemana: Buenos, Argentina, 1996; Chapter 10. Available online: hhttps://www.conicet.gov.ar/new_scp/detalle.php?keywordsamp;id=20994amp;libros=yesamp;detalles=yesamp;lib_id=761727 (accessed on 20 December 2024).
46. Beck, H.E.; Zimmermann, N.E.; McVicar, T.R.; Vergopolan, N.; Berg, A.; Wood, E.F. Present and future Köppen-Geiger climate classification maps at 1-km resolution. *Sci. Data* **2018**, *5*, 180214. [CrossRef] [PubMed]
47. Marquez, J.; Martinez Carretero, E.E.; Dalmasso, A.D. Provincias fitogeográficas de la Provincia de San Juan. Repositorio Institucional CONICET Digital, 2016; pp. 187–197. Available online: https://ri.conicet.gov.ar/handle/11336/129240 (accessed on 20 December 2024).
48. European Commission, Joint Research Centre (JRC). South America Mean Annual Precipitation Map (TRMM 3B43 dataset). *European Commission, Joint Research Centre (JRC) [Dataset] PID.* 2015. Available online: http://data.europa.eu/89h/3950386f-1b43-4247-8d99-40dd89f164a3 (accessed on 23 December 2024).
49. Instituto Geográfico Nacional. Atlas Nacional Interactivo de Argentina [en línea]. Available online: https://www.ign.gob.ar/NuestrasActividades/Geodesia/ModeloDigitalElevaciones/Mapa (accessed on 5 January 2022).
50. Conrad, O.; Bechtel, B.; Bock, M.; Dietrich, H.; Fischer, E.; Gerlitz, L.; Wehberg, J.; Wichmann, V.; Böhner, J. System for Automated Geoscientific Analyses (SAGA) v. 2.1.4. *Geosci. Model Dev.* **2015**, *8*, 1991–2007. [CrossRef]
51. Strahler, A.N. Quantitative geomorphology of drainage basins and channel networks. In *Handbook of Applied Hydrology*; Chow, V.T., Ed.; McGraw-Hill: New York, NY, USA, 1964; pp. 4–39.
52. QGIS.org. *QGIS Geographic Information System*. QGIS Association. 2024. Available online: https://www.qgis.org/ (accessed on 23 December 2024).
53. Map Data ©Google. 2015. In QuickMapServices Version 0.19.33. Developer: NextGIS. Available online: https://www.google.at/permissions/geoguidelines/attr-guide.html (accessed on 23 December 2024).
54. Horton, R.E. Erosional development of streams and their drainage basins; hydrophysical approach to quantitative morphology. *Geol. Soc. Am. Bull.* **1945**, *56*, 275–370. [CrossRef]
55. Horton, R.E. Drainage-basin characteristics. *Trans. Am. Geophys. Union* **1932**, *13*, 350–361.
56. Miller, V.C. *A Quantitative Geomorphic Study of Drainage Basin Characteristics in the Clinch Mountain Area*; Virginia and Tennessee, Proj. NR, Technical Report; Columbia University: New York, NY, USA, 1953; pp. 389–402.
57. Schumm, S.A. Evolution of Drainage Systems & Slopes in Badlands at Perth, New Jersey. *Bull. Geol. Soc. Am.* **1956**, *67*, 597–646. [CrossRef]
58. Hadley, R.; Schumm, S. *Sediment Source and Drainage Basin Characteristics in Upper Cheyenne River Basin*. US Geological Survey Water Supply Paper: 1961; 1531-B. Available online: https://www.semanticscholar.org/paper/B.-Sediment-Sources-and-Drainage-Basin-Character%C2%AD-Culler-Hadley/2c5c3e31a212b3a22e2719827c4f771d2418c00d (accessed on 23 December 2024).

59. Gravelius, H. Grundrifi der gesamten Gewcisserkunde. In *Band I: Flufikunde Compendium of Hydrology*; Goschen: Berlin, Germany, 1914; Volume I. Rivers. (In German)
60. Santi Malnis, P.; Colombi, C.E.; Rothis, L.M.; Alcober, O. Fluvial architecture and paleoenvironmental evolution of the Los Colorados Formation (Norian): Postrift stage of the Ischigualasto–Villa Unión Basin, NW Argentina. *J. Sediment. Res.* **2020**, *90*, 1436–1462. [CrossRef]
61. Schencman, L.J.; Colombi, C.; Santi Malnis, P.; Limarino, C.O. Diagénesis y procedencia de la Formación Los Colorados (Noriano), Cuenca de Ischigualasto-Villa Unión, Noroeste de Argentina. *Rev. Asoc. Geológica Argent.* **2015**, *72*, 219–234.
62. Hamilton, N.E.; Ferry, M. ggtern: Ternary Diagrams Using ggplot2. *J. Stat. Softw. Code Snippets* **2018**, *87*, 1–17. [CrossRef]
63. Wickham, H. *ggplot2: Elegant Graphics for Data Analysis*; Springer: New York, NY, USA, 2016.
64. Zeileis, A.; Köll, S.; Graham, N. Various Versatile Variances: An Object-Oriented Implementation of Clustered Covariances in R. *J. Stat. Softw.* **2020**, *95*, 1–36. [CrossRef]
65. Wickham, H.; François, R.; Henry, L.; Müller, K.; Vaughan, D. dplyr: A Grammar of Data Manipulation. R Package Version 1.1.4. 2023. Available online: https://CRAN.R-project.org/package=dplyr (accessed on 23 December 2024).
66. Kassambara, A.; Mundt, F. factoextra: Extract and Visualize the Results of Multivariate Data Analyses. R Package Version 1.0.7. 2020. Available online: https://CRAN.R-project.org/package=factoextra (accessed on 23 December 2024).
67. Fox, J.; Weisberg, S.; Price, B. carData: Companion to Applied Regression Data Sets. R Package Version 2022 3.0-5. Available online: https://CRAN.R-project.org/package=carData (accessed on 23 December 2024).
68. Meyer, D.; Dimitriadou, E.; Hornik, K.; Weingessel, A.; Leisch, F. e1071: Misc Functions of the Department of Statistics, Probability Theory Group (Formerly: E1071), TU Wien. R Package Version 1.7-14. 2023. Available online: https://CRAN.R-project.org/package=e1071 (accessed on 23 December 2024).
69. Charrad, M.; Ghazzali, N.; Boiteau, V.; Niknafs, A. NbClust: An R Package for Determining the Relevant Number of Clusters in a Data Set. *J. Stat. Softw.* **2014**, *61*, 1–36. Available online: http://www.jstatsoft.org/v61/i06/ (accessed on 23 December 2024). [CrossRef]
70. Genz, A.; Bretz, F. *Computation of Multivariate Normal and t Probabilities*; Series Lecture Notes in Statistics; Springer: Berlin/Heidelberg, Germany, 2009; ISBN 978-3-642-01688-2.
71. Simko, V.R.; Wei, T. Package 'corrplot': Visualization of a Correlation Matrix (Version 0.92). 2021. Available online: https://github.com/taiyun/corrplot (accessed on 23 December 2024).
72. Wickham, H.; Miller, E.; Smith, D. Haven: Import and Export 'SPSS', 'Stata' and 'SAS' Files. R Package Version 2.5.3. 2023. Available online: https://CRAN.R-project.org/package=haven (accessed on 23 December 2024).
73. Fox, J.; Marquez, M. RcmdrMisc: R Commander Miscellaneous Functions. R Package Version 2.9-1. 2023. Available online: https://CRAN.R-project.org/package=RcmdrMisc (accessed on 23 December 2024).
74. Kassambara, A. rstatix: Pipe-Friendly Framework for Basic Statistical Tests. R Package Version 0.7.2. 2023. Available online: https://CRAN.R-project.org/package=rstatix (accessed on 23 December 2024).
75. Thant, A.A.; Aye, S.M.; Mandalay, M. Euclidean, manhattan and minkowski distance methods for clustering algorithms. International Journal of Scientific Research in Science. *Eng. Technol.* **2020**, *7*, 553–559.
76. Rodrigo, J.A. Clustering y Heatmaps: Aprendizaje no Supervisado. 2017. Available online: https://rpubs.com/JoaquinAR/310338 (accessed on 23 December 2024).
77. Aldás Manzano, J.; Uriel Jiménez, E. *Análisis Multivariante Aplicado con R*, 2nd ed.; Ediciones Paraninfo SA: Madrid, Spain, 2017; p. 669.
78. Cabrera, A.L. Regiones fitogeográficas argentinas. In *Enciclopedia Argentina de Agricultura y Jardinería*, 1st ed.; Tomo, F., II, Ed.; ACME: Buenos Aires, Argentina, 1976; pp. 1–85.
79. Morello, J.; Protomastro, G.; Sancholuz, L.; Blanco, C. Estudio Macroecológico de Los Llanos de La Rioja. *Rev. IDIA* **1977**, *34*, 242–248.
80. Page, S.; Limarino, C.O.; Caselli, A. Basaltos alcalinos en el Triásico de la Cuenca Ischigualasto-Villa Unión, provincias de La Rioja y San Juan. *Rev. Asoc. Geológica Argent.* **1997**, *52*, 202–208.
81. Gulbranson, E.L.; Ciccioli, P.L.; Montañez, I.P.; Marenssi, S.A.; Limarino, C.O.; Schmitz, M.D.; Davydov, V. Paleoenvironments and age of the Talampaya Formation: The Permo-Triassic boundary in northwestern Argentina. *J. S. Am. Earth Sci.* **2015**, *63*, 310–322. [CrossRef]
82. Colombi, C.E.; Limarino, C.O.; Alcober, O.A. Allogenic controls on the fluvial architecture and fossil preservation of the Upper Triassic Ischigualasto Formation, NW Argentina. *Sediment. Geol.* **2017**, *362*, 1–16. [CrossRef]
83. Rivarola, D.; Spalletti, L. Modelo de sedimentación continental para el rift cretácico de la Argentina central: Ejemplo de la sierra de las Quijadas, San Luis. *Rev. Asoc. Geológica Argent.* **2006**, *61*, 63–80.

84. Santi Malnis, P.; Rothis, L.M.; Colombi, C.E. *Distributary Drainage Systems in La Huerta Range, Westerm Pampean Ranges, San Juan, Argentina*; Advances in Geomorphology and Quaternary Studies in Argentina: Special Symposium from the Argentine Association of Geomorphology and Quaternary Studies; Springer International Publishing: Cham, Switzerland, 2020; pp. 136–157. [CrossRef]
85. Nichols, G.J.; Fisher, J.A. Processes, facies and architecture of fluvial distributary system deposits. *Sediment. Geol.* **2007**, *195*, 75–90. [CrossRef]
86. Hartley, A.J.; Weissmann, G.S.; Nichols, G.J.; Warwick, G.L. Large distributive fluvial systems: Characteristics, distribution, and controls on development. *J. Sediment. Res.* **2010**, *80*, 167–183. [CrossRef]
87. Damanti, J.F.; Geomorphic and structural controls on facies patterns and sediment composition in a modern foreland basin. In Alluvial Sedimentation. 1993; pp. 219–233. Available online: https://onlinelibrary.wiley.com/doi/book/10.1002/9781444303995 (accessed on 23 December 2024).
88. Santamaria, A.; Santi Malnis, P.; Bertona, M.D.; Rothis, L.M.; Pures, T.S. Geomorfología y facies sedimentarias del mega-abanico del río Huaco, Cuenca del Bermejo, San Juan, Argentina. *Lat. Am. J. Sedimentol. Basin Anal.* **2023**, *30*, 139–161.